

Abstract

SPEAKER, DANIEL. Monte Carlo Application for the use of Detector Response Function on Scintillation Detector Spectra. (Under the direction of Dr. Robin P. Gardner).

The Detector Response function (DRF) is the pulse height distribution for an incident radiation, and is also a PDF which has the properties of always being greater than or equal to zero and also integrates to unity. The application of the DRF on a simulated spectrum results in the benchmarking of the simulation results with experimental results. The results obtained are Gaussian shapes that are caused by the statistical fluctuations in the energy and collection efficiency of the detector. To find the perfect simulation of the DRF is impossible due to the fact that the detector might have imperfections, where electrons can essentially become trapped and not be collected. Instead, one must rely on empirical models of nonlinearity and simulation data.

This is what CEAR's DRF code G03 accomplishes. The reason G03 is so time consuming is because it runs through every particle individually with all of its primary and tertiary interactions. In most other Monte Carlo simulations, more rigorous electron transport is used; however, it makes the code more computationally expensive. G03 couples rigorous gamma ray transport with very simple electron transport. The non-linearity and the variable flat continua part of the DRF is accounted for by using this methodology. This Monte Carlo simulation also simulates and incorporates the detector as a bare crystal. It was found that this could account for as much as 5 percent of a reduction of the incident energy as well as distort the response function in the lower energy range of the function. For this goal, MCNP was employed to simulate the difference between the bare and covered crystal. From these results of the simulation of

the protective can and no can simulation, the pulse height spectra are different in different regions of the spectra. This variance causes a sizeable difference in valley region, which can be explained as many different photopeaks in the valley region due to Compton scatters in the can. Also, one can distinguish between the plots and conclude that the side of the can contributes to the continuum due to the backwards continuum which starts around 0.2 MeV.

For the electrons in the front and the side, the spectrum will be run through a Monte Carlo program that will calculate the energy deposited into the crystal. But, as will be shown, the electrons only need to be accounted for high resolution detectors such as a BGO detector. Perhaps the most significant photos, those from the front, will be added by G03 having a spectrum of incident photons on the crystal instead of the utilizing a monoenergetic energy, which is how it is done now. Implantation of all the above phenomena into G03 will be accomplished.

Monte Carlo Application for the Use of Detector Response Function on
Scintillation Detector Spectra

by
Daniel Phillip Speaker

A thesis submitted to the Graduate Faculty of
North Carolina State University
in partial fulfillment of the
Requirements for the Degree of
Master of Science

Nuclear Engineering

Raleigh, North Carolina

2009

APPROVED BY:

Dr. Robert E. White
Committee Member

Dr. Hany S. Abdel-Khalik
Committee Member

Dr. Robin P. Gardner
Chair of Advisory Committee

Biography

Daniel P. Speaker was born in Dallas, TX, in May of 1978. He is the youngest of three children. His primary education began in the Dallas ISD public schools and ended with his graduation from Bishop Lynch Catholic High School in Dallas, TX. He began his college education at Brookhaven Community College in Dallas, TX, and completed his Bachelor of Science degree at Texas A & M University in College Station, TX, in December of 2004.

After graduating from Texas A&M, Daniel worked as a intern in the LANCE facility at Los Alamos National Lab. He began his graduate studies at North Carolina State University in August of 2005 and continued through to the completion of his Master of Science degree in nuclear engineering.

Acknowledgements

To my friends everywhere who have shared in many fun and enlightening experiences. To the Garden Place Cul de Sac and Jersey who reminded me of where I came from.

To my friends back in my hometown, Dallas, who taught me what real friendship as well as what engineering really means.

To Alan Walter, whose passion fueled my fire to become a nuclear engineer.

To my family: My brother, Paul, who has always been my mentor. My sister who showed me that one can do everything with heart, my stepfather Alex always supported me in every way, my mom for being my best friend and my father for his lessons on life.

I dedicate this work to my classmates and comrades at NCSU who were patient and taught me a lot about the balance that one must accomplish between work and one's real life. Most especially to Ross Hays, Alan Rominger, and Thomas Holmes, without whose help this work would not have been possible.

To Dr. Robin P. Gardner who gave me a way to accomplish my hopes and dreams.

However, this work, in its totality, is dedicated to my wife, Joy. Without her, this work would have had no heart and I, neither happiness, nor sanity.

Table of Contents

List of Figures.....	v
List of Tables.....	vii
1 Introduction to Detector Response Functions (DRF's) and previous work.....	1
2 CEAR Applications of the DRF	9
3 Inherent Problems with G03 and Motivation for Its Modification.....	15
4 MCNP Simulation of Can Phenomena.....	20
5 Implantation of Simulated Phenomena into G03.....	32
6 Results.....	43
6.1 Overall Statement of Detector Parameters and Preliminary Results.....	43
6.2 Heath can data final.....	51
6.3 16"x4"x2" Sodium Iodine Portal Monitoring Detector.....	54
6.4 G03 Results.....	56
7 Discussion and Conclusions.....	57
8 References.....	58

List of Figures

Figure 1: Part of an MCNP detector unspread response function for Sodium Iodide (NaI).	5
Figure 2: Components of the detector response function for Ge Detector	8
Figure 3: Illustration of the four features described of a Si(Li) semiconductor detectors	10
Figure 4: Photoelectric Effect Cross Sections for many types of detectors.....	11
Figure 5: Photoelectric Effect Cross Sections Zoomed in.....	12
Figure 6: Compton (Incoherent) Scattering Cross Sections for many types of detectors.....	12
Figure 7: Pair Production Cross Sections for many types of detectors.....	13
Figure 8: Background of radioactivity coming from the lanthanum part of La ₃ Br	18
Figure 9: Heath can schematic	21
Figure 10: Percentage of photons going through the front of the detector can that are not being attenuated for Heath 3x3	23
Figure 11: Photon spectrum incident on the crystal after being attenuated through the can	23
Figure 12: Electron spectrum incident on the crystal after being attenuated through the can	24
Figure 13: Compton interactions with the whole protective can (wwc), without the can (woc), and with just the front face (wc).....	25
Figure 14: Auger interactions with the whole protective can (wwc), without the can (woc), and with just the front face (wc)	25
Figure 15: NaI Unspread spectra	26
Figure 16: BGO Unspread spectra.....	26
Figure 17: LaBr Unspread spectra	27
Figure 18: Electron spectrum bouncing back into the detector from the side	29
Figure 19: Photon spectrum bouncing back into the detector from the side	29
Figure 20: Electron spectrum incident on the crystal after being attenuated through the can	30
Figure 21: Photon spectrum incident on the crystal after being attenuated through the can	30
Figure 22: St. Gobain 16"x4"x2" NaI Detector.....	31
Figure 23: Typical Detector Housing for all produced 2x2 Cylindrical Detector	32
Figure 24: Cesium spectra point wise after attenuated through the front of the protective can	34
Figure 25: Unspread spectra for Cesium Unshifted spectra from G03.....	35
Figure 26: Per source particle of photons coming back into the crystal from the side.....	36
Figure 27: Light yield for various detectors	40
Figure 28: Light Yield for La ₃ Br	41
Figure 29: NaI 3x3 Heath 0.662 MeV	43
Figure 30: Heath can for different size NaI detectors Without Detector Housing for 2.614 MeV	44

Figure 31: Heath can for different size NaI detectors With Detector Housing (Can) for 2.614 MeV	44
Figure 32: With Heath can, different types of 3x3 Detectors for 0.662 MeV	45
Figure 33: With Heath can, different types of 3x3 Detectors for 0.662 MeV	45
Figure 34: With Heath can, different types of 3x3 Detectors for 7 MeV	46
Figure 35: With Heath can, different types of 3x3 Detectors for 7 MeV	46
Figure 36: Compton interactions for various detector types, and without the protective can	47
Figure 37: Compton interactions for various detector types, and with the protective can	47
Figure 38: 3x3 LaBr detectors at 0.662 incident energy 256 channels with Heath can	48
Figure 39: 3x3 LaBr detectors at 1.332 incident energy 256 channels with Heath can	48
Figure 40: 3x3 LaCl detectors at 0.662 incident energy with Heath can and 256 channels.	49
Figure 41: 3x3 LaCl detectors at 1.332 incident energy with Heath can and 256 channels... ..	49
Figure 42: 3x3 BGO detectors at 0.662 incident energy	50
Figure 43: 3x3 BGO detectors at 1.332 incident energy and 256 channels.....	50
Figure 44: Photon front for 3x3 NaI 1002 channels with Heath can for selective energies for clarity.....	51
Figure 45: Electron Front for 3x3 NaI 1002 channels with Heath can.....	51
Figure 46: Photon side for 3x3 NaI 1002 channels with Heath can	52
Figure 47: Photon side for 3x3 NaI 1002 channels with Heath can zoomed in.....	52
Figure 48: Electron side for 3x3 NaI 1002 channels with Heath can	53
Figure 49: Pulse height with out can side for 3x3 NaI 1002 channels with Heath can	53
Figure 50: Pulse Height with whole can side for 3x3 NaI 1002 channels with Heath can... ..	54
Figure 51: Photons in front for Raytheon box 16"x4"x2"	54
Figure 52: Percentage of uncollided flux.....	55
Figure 53: Pulse Height with whole can	55
Figure 54: The affect of Photon spectra the pulse Height, and the showing of error in spreading the spectrum outside the code	56
Figure 55: The affect of Photon spectra from the pulse height with MCNP and G03	56

List of Tables

Table 1: Gaussian Spreading Parameters from the original G03.....	37
---	----

1 Introduction to Detector Response Functions (DRF's) and Previous Work

As the world grows ever more efficient with computer technology and hardware for radiation detection systems, the application of the detector response function is going to become ever more important in the development of a myriad of things - from helping the security of this country be more secure to helping imaging of cancer treatment and making this treatment more efficient. The mathematical definition of the detector response function is the pulse height spectrum that results from the incidence of monoenergetic photon energy, E . The response function is also defined as being caused by the detector in the energy range of interest (Gardner, 2005). The photon energies of interest in that range can be divided evenly or not. Technically the proper way of defining the DRF is a two-dimensional matrix that is of an $n \times n$ rank, matrix with the columns and vectors of the $n \times n$ signifying photon incident on the detector face of can (made of aluminum and other materials, discussed later) and the number of channels. An easy way of think about the definition of the detector response function is being the interaction that only happens in the detector and what the detector is comprised of. It is as if nothing else existed and you have a source with many discrete photon energies and they are picked up at monoenergetic energy from the detector that has nothing around it. Affects that are commonly mistaken for parts of the detector response function, a perfect DRF has no air to scatter the radiation, include shielding between and around the source and detector, Air and other particulates between the source and detector. This is due to Compton Scattering interactions between the distance from the detector, and all the constituents of what is between. This is a commonality is that shielding response around the detector- source

setup is included. As an example, when in the Heath experiments, a misconceived notion is that the response from the shielding materials causes peaks in the Compton Continuum are a part of the DRF. This is not a part of the DRF. Moreover there was scattering from the source stand (Heath, 1964). But nevertheless it is a very good model to be followed. In the results section G03 is benchmarked against these Heath experiments.

The point that needs to be stressed is that at our present level of technology we cannot provide a perfect, or ideal, response function that works for all detectors of the same model. This is due in part because the probability of growing the exact same crystal with no imperfections is impossible to replicate two times, much less in mass production. Another thing is that different detectors of the same composition and dimensions are made with different container walls (which protect the inside crystal) by different companies and the same company at different times, which is one of the main points of this work. Cracks or impurities that are added to the crystal by exposure to radiation can channel or trap the electrons, which can greatly affect the Compton continuum region. For a good high resolution elemental analysis, such small details are critical for measurements that reveal elemental type and amount. But the basic analysis of today yields first-order accuracy that can be used with somewhat less accuracy. Also note that the cross sections of a perfect crystal for electron transport are unknown, so Monte Carlo computer codes cannot be used directly for the complete simulation of detector response functions since electron transport is also important.

The advantages of the implementation of DRF's are many; and in the way of helping with the speed of the process, DRF's serve as a significant variance reduction

approach in Monte Carlo codes that calculate photon spectra. For software recognition purposes, the DRF has a natural smoothing effect. Still yet, there are phenomena that are not considered, such as the detector can, the photomultiplier tube, and the collection efficiency for the perfect detector. To impose a different layer of library spectra that represents an element of a particular thickness of material of the detector with the typical and predicted responses from the detector can be a powerful tool for many uses. If one looked at a very high resolution detector and looked at the most minute part of the spectra in the spaces in between the photopeaks. These parts of the spectra consist of orders of magnitude of the source particle in the range of 1 of 10,000, which is a very low yield in the total spectrum. With the tiny constituents of the spectrum, one can find elemental compositions of any elements with a perfect detector. This is what CEARXRF does but with low energy photons and semiconductor materials, which is a more complicated problem than G03 deals with. This is due to the fact that at low energies the photoelectric effect dominates, and there is not many Compton interactions taking place hence less nonlinearities in the light collection.

There are three ways, documented by Gardner, Yacount, Zhang, and Verghese, (1986) to obtain detector response functions. One is completely experimental, where one obtains the response in the matrix from a large number of measured monoenergetic spectra and interpolates for other energies. The Heath experiments described before are examples of this. But this, which was stated earlier, is not exactly a response function in the clear definition of the word. This is because the lead around the source and detector

and source stand add parts to the spectrum that are not part of the classic definition of the DRF. But this type of data is essential for the benchmarking of any simulated DRF.

Another way is entirely by Monte Carlo simulation. A basic example of a Monte Carlo process would be a program which randomly picks a number from 1 through 4 a certain number of times or samples, call it number of samples (n). If n was very large, one can see that there would be near even one-quarter probability of the program to pick one of the numbers. If the n sample size, of was let's say 3, than it would dictate that one number could never be picked, and with the possibility of more than one. In this approach for the DRF one generates response functions by simulation for a large number of monoenergetic photon energy. Later on a MCNP simulation, which is a very exotic Monte Carlo program, is run and data is obtained to add some new components of the DRF. To see what we have talked about visually, below in Figure 1 is an example of an MCNP spectrum that is a DRF that is ranged from 0.3443 to 1.173 MeV. This data is not spread to account for the collection efficiency and imperfections in the detector crystal, which in this case is Sodium Iodide (NaI). One can easily see the Compton edge sharply. Other features such as the x-rays from Iodide near the photopeak. The photopeak is one channel of 1000, which is a purely simulation work. This would correspond to the perfect detector, without the electronic effect that causes the Gaussian spreading.

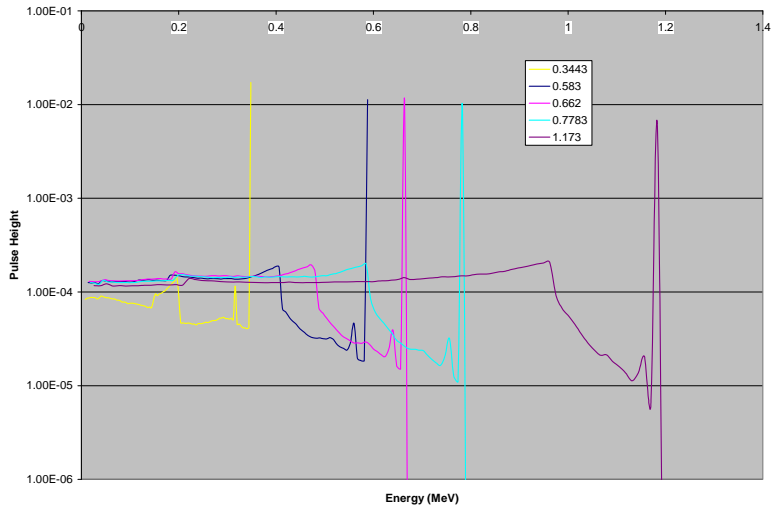


Figure 1: Part of an MCNP detector unsread response function for Sodium Iodide (NaI)

Others, such as Campbell (1990), have tried to model the parts of the DRF that are important in the range of interest, in his case low x-ray energies. In one such paper Campbell added the response of the diodes as part of a (Si)Li drifted detector. All the components, all the continuants of the semiconductor is calculated separately and then added up. Some other codes have focused on speed of the generation of DRF. In one such instance, GADRAS at Sandia National Lab led by Mattingly (Mattingly, 2008), has produced a very fast DRF code by using a one dimensional approach. The components are calculated separately and then added up and then spread as in G03, but the Compton part is the interesting because in 1 dimensional coordinates this response would be unable to be calculated. This is done by empirical sampling to obtain that part of the response.

The third and the final approach is the semi-empirical approach. This is where one determines an analytic model and uses least squares fits to a smaller number of single

energy results and processes and then generalizes these results with energy to provide a continuous model. An example of one of these processes is provided in the code that this thesis deals with in modeling the detector response functions, G03. This process is a set of functions that is used for the three photon cross sections in a detector that is of interest. In this way a search of cross sections in this way is more efficient than a tabular form, like that found in MCNP. The reason why a semi-empirical approach is chosen and preferred for some applications is that one does not for example need to model the *exact* straggling of the electron. When one considers straggling in electron transport into a MCNP deck, the time is increased ten fold and the accuracy is also poor because one does not have the cross sections required for electron transport in single crystals. By using an empirical relationship that adequately simulates the energy deposited, the code will be faster, hence more efficient, and much more accurate.

Many authors, including Campbell (1990), devoted much time to producing specific key features to the detector response functions. Figure 2 is a semiconductor's components of the DRF, which is beyond the range of this work, but nevertheless it is still instructive in showing various components of the DRF. The reason for this is that although some parts of the DRF for both semiconductors and scintillation detectors have commonalities, the basic charge collection and detector components differ in that the two and have entirely different components for the DRF.

This is why on the onset of this code's development it was proposed by Sood and Gardner (2004) to use Monte Carlo simulation to obtain certain of the different components of the DRF. By finding all the components of the spectra and then adding

them together yields the entire spectrum. This is the central theme of this thesis is that using a semi-empirical method one can generalize and make slight changes in the code. This was also accomplished at a great expense to preserving the speed of the code. By G03's nature it is simple so in return it is fast, but also easy to manipulate. The trick is in compiling huge amounts of data and putting it into a semi-empirical model to preserve its simplicity. An important note is that accuracy suffers. This is due to the fact that, as will be explained later, G03 runs more computationally efficient by using functional vs. a tabular acquisition of data. The components added are that of the protective detector housing, which can constitute around 5% of the total spectrum.

The components are first of all, the most recognizable, the Gaussian standard deviation of the full energy peak. This applies as well to the entire spectrum. The exponential tails and the flat continua are also simulated. The flat continuum is produced because whenever a photoelectron is caused by a photoelectric effect it has an even probability to deposit its energy. The reason for this is geometry. Let us say you have 1 interaction with two very different effects in the same place lets say at the corner of the crystal. The first interaction a Compton interaction happens and the electron escapes without depositing much of the energy, we will call this A. The second one happens at the same location but the Compton scatter and the electron deposits the full amount of the energy by evacuating thru the opposite corner, depositing a lot or all of its energy, call it B. A is the left side of the flat continua and B is the right side. If one really thinks about it playing all the scenarios or samples in your mind, it makes sense why it is flat. The part labeled 5 in the picture represents multiple Compton scatters, before absorption. The one

on top is secondary and the bottom part is the tertiary reactions, which represents possibly many progeny of Compton scatters. It would make since the tertiary reactions contribution to the spectrum span more of an energy range then the secondary reactions.

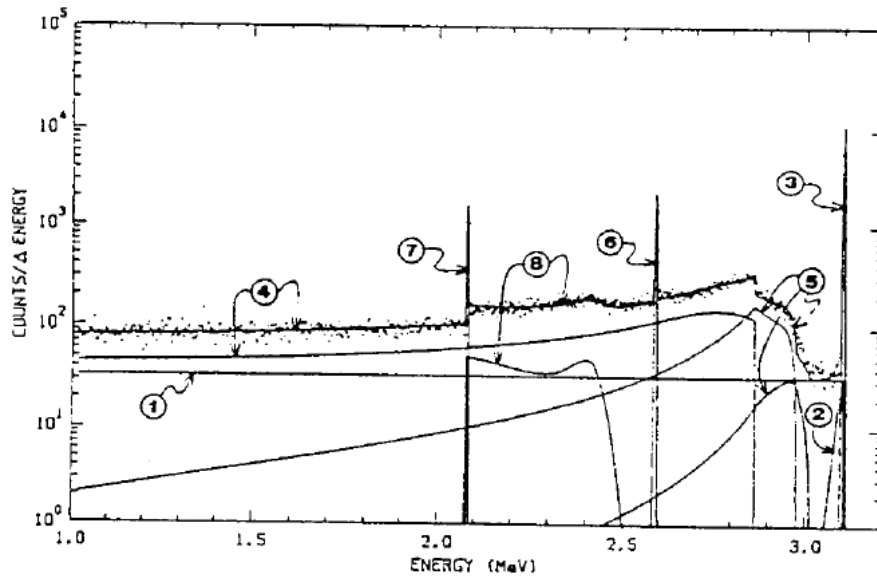


Figure 2: Components of the detector response function for Ge Detector (1) the flat continuum, (2) the exponential tail, (3) the full energy peak, (4) the Compton electron scattering continuum, (5) a continuum between the Compton electron scattering continuum and the full energy peak, (6) the single escape peak, (7) the double escape peak, (8) a small scattering continuum between the single and double escape peaks (Y. Jin, R. P. Gardner, and K. Verghese, 1986).

2 CEAR Applications of the DRF

The Center for Engineering Applications of Radioisotopes at North Carolina University has been investigating DRF for more than three decades. The first few attempts for CEAR to unlock a DRF were in semiconductor materials. In the late 70's, Gardner, Wielopolski, and Verghese (1977) published a paper where the use of the Monte Carlo method was employed for extending the fundamental parameters of x-rays. This means they used a semi-empirical approach. The purpose of this was to find elemental amounts of materials by use of the library least squares method with an energy dispersive X-ray fluorescence analysis systems. The mathematical models for components of the response function were in the preliminary stages. In this stage of computer processor development, huge computers did the same job that a microprocessor does today. The limitation was computation and it was suggested that experimental methods should be exploited to speed up response function simulation with many variations of sample. In CEAR's second attempt, accomplished by Wielopolski and Gardner, four spectral features were found in the X-ray energy region. These were the flat continuum, the exponential tail to the left of each photopeak, the X-ray escape from Silicon, and the Gaussian photopeak. The models of these equations are shown below in equations 2.1-2.3. The expressions for each feature are shown, split up, in Figure 3.

$$C(E', E, \sigma) = A_1(E)F(E', E, \sigma) \quad (2.1)$$

$$T(E', E, \sigma) = A_2(E) \exp[-A_3(E)E']F(E', E, \sigma) \quad (2.2)$$

$$G_E(E', E, \sigma) = (2\pi)^{1/2} \sigma^{-1} \exp[-(E'-E)^2 / 2\sigma^2] \quad (2.3)$$

Where E is the incident photon energy, E' is the pulse height energy, the A 's are experimental constants, the $F(E', E, \sigma)$ are given by (Wielopolski and Gardner, 1979):

$$F(E', E, \sigma) = \int_{E'}^{\infty} G(E'', E, \sigma) dE'' \quad (2.4)$$

And shown explicitly in equation 2.5:

$$F(E', E, \sigma) = (1/2) \operatorname{erf}[(E' - E) / \sqrt{2\sigma}] \quad (2.5)$$

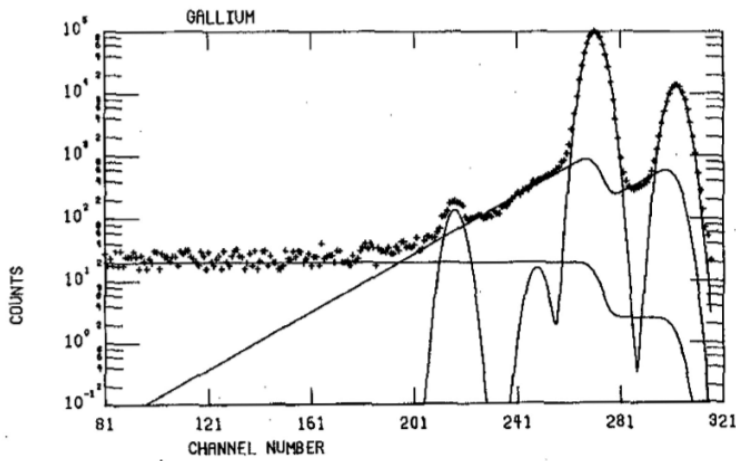


Figure 3: Illustration of the four features described of a Si(Li) semiconductor detectors (L. Wielopolski and R. P. Gardner, 1979)

Much work was done in the area of semiconductor materials for CEAR. As recently as 2008, Fusheng Li has improved the X-ray code using the detector response function with a GUI interface that provides very useful results or elemental identification for x-rays. But the scintillation prediction of the DRF is more complex for many reasons. The components of the DRF in semiconductors are easier to predict. One of these reasons

is that x-ray spectra are at the low keV range, which means that you have a higher probability of photoelectric absorption. And, in this interaction, one only has to track the electron until it deposits its energy in the crystal. This is because you do not have to predict secondary and tertiary interactions in semiconductors. In scintillation detectors, spectra of up to many MeV are used in experiments, but are rarely used in sub-keV applications. At these ranges of energy, Compton Scatters have a higher probability of happening, which is apparent below. It is important to also note that NaI is more nonlinear than a higher effective Z detector such as LaBr₃. Utilizing data from figures 4 through 7, it the belief this is because there is higher probability of Compton Scatter in the mid-range energies.

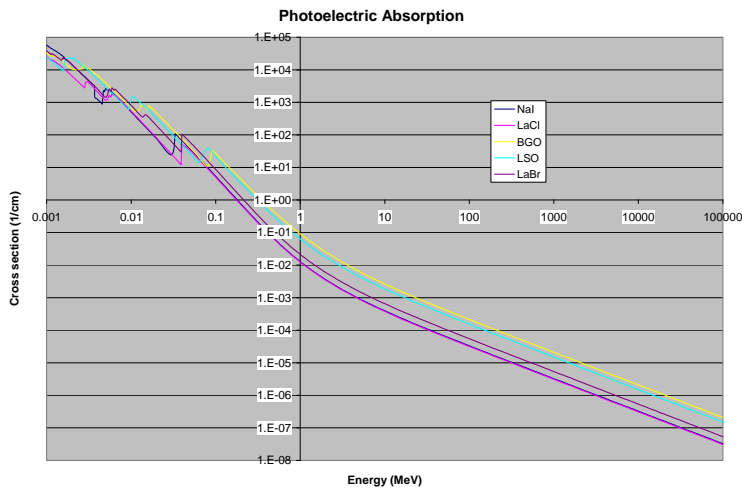


Figure 4: Photoelectric Effect Cross Sections for many types of detectors.

Element/Compound/Mixture Selection, from NIST XCOM website.

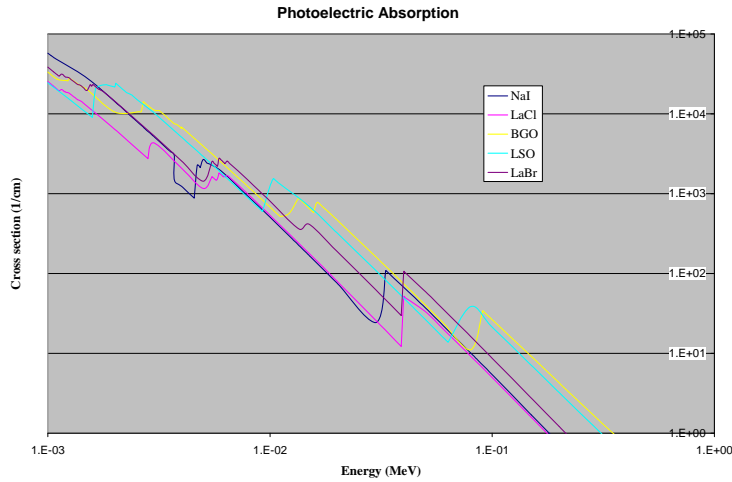


Figure 5: Photoelectric Effect Cross Sections Zoomed in. Element/Compound/Mixture Selection, from NIST XCOM website

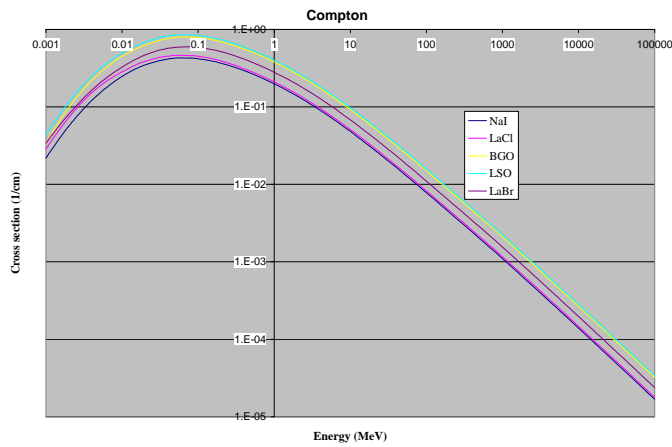


Figure 6: Compton (Incoherent) Scattering Cross Sections for many types of detectors. Element/Compound/Mixture Selection, from NIST XCOM website.

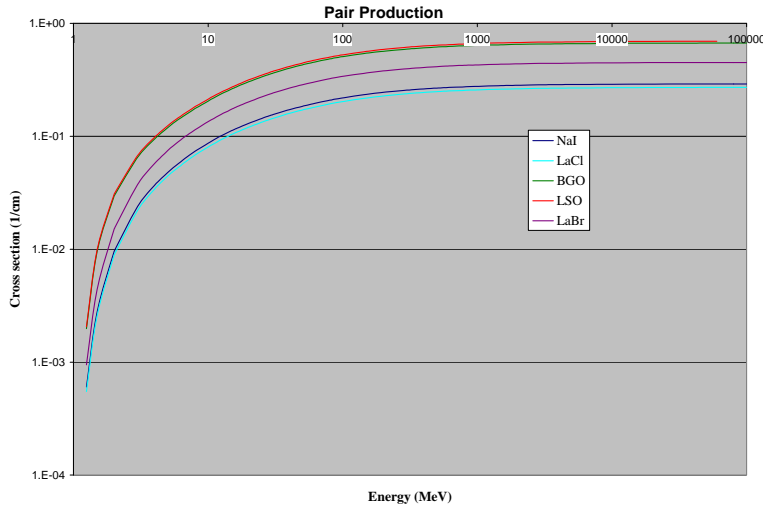


Figure 7: Pair Production Cross Sections for many types of detectors.

To further complicate matters, there is also a higher probability of pair production for the range of energies for which scintillation detectors are applicable. So, annihilation photons must be tracked as well. In a code like MCNP, complicated electron models are employed to get the pulse height for a detector volume. This can multiply the computation time more than 10 fold.

CEAR started studies in the early 1990's to tackle this difficult problem of the scintillation DRF. In the code named DRFNCS, a semi-empirical approach was employed to calculate detector responses for many energies of photons incident on the crystal. This code is the very beginnings of G03, which is the code to which the improvements are to be made. Much of the geometry tracking done in the present G03 is used exactly the same way it was in the 1990's, with some optimizations for time. Berger and Seltzer (1972) cited that the addition of the Bremsstrahlung radiation contribution to the DRF would yield a large difference in the spectra. In DRFNCS, as in the present

code, the electron had a simple range relationship that is shown in equation 2.7. This enables the code to run very fast.

$$R_e = \frac{aE^{(b-c \ln E)}}{\rho} \quad (2.6)$$

The code also used basic photon interactions such as pair production, Compton Scattering, and photoelectric effect, and excluded unnecessary interactions such as Rayleigh scattering. The photoelectric effect assumes isotropic scattering for the photoelectron. The Compton Scattering is treated with the standard Klein-Nishina formula and the Kahn rejection technique (Kahn, 1954) was applied to select an energy and subsequent scatter direction. The pair production interaction assumed an isotropic distribution of the electron and positron with a minimum angle θ_m , shown below as:

$$\theta_m = \frac{m_o c^2}{h\nu} \quad (2.7)$$

This study yielded some interesting and accurate data. The problem, when comparing it to the experiment, is that there are large variances in the valley region as well as discrepancies in the Compton Continuum in the present G03 that will be shown later.

3 Inherent Problems with G03 and Motivation for Its Modification

G03 is a very useful tool for calculating response functions for some detectors. The Center for Engineering Applications of Radioisotopes, CEAR, is looking to use these response functions to produce radioisotope (or elemental) library spectra to help with Homeland Security in order to make the inspection of cargos at seaports and at our borders more efficient and more accurate. In order to convolve simulated radioisotope photon and neutron spectra of different yields and types, one must look at all parts of the spectra. In addition, the response function could be applicable in concert with the elemental analysis of many composite compounds between the source and detector, especially when considering high resolution detectors such as lanthanum and germanium detectors.

However, there are some developments G03 has to hurdle. The analyses of G03, in its current phase, needs to be accomplished in all parts of the spectra and accuracy are important. Simulated spectra that are orders of magnitude differentiated by use with and without the protective can around it, may lead to as much as 0.001- 0.0001% difference in the normalized intensity of the photopeak. These are things that must be observed and changed regarding this approach to the detector response function.

- Any Monte Carlo code will never have a perfect representation of a detector response function for any type of detector. This is due to the fact that every detector is different: from the differing compositions of the cans being used, to effects from crystals grown that have not yet been actually modeled at this time, to imperfections of the crystal, which result in insufficient charge collection.

- The detector is a bare crystal. Avneet Sood's thesis (2000) has stated that the addition of the front face of the can would contribute to the improvement on yield in the valley region. It is also evident, which will be shown later, that the side detector crystal covering contributes to slight fluctuations in the Compton Continuum energy range. There is also a possibility that the PMT, at high incident photon energies, can affect the spectra. CEAR provides new features of the detector response function and, in doing the modification of G03, will provide more accuracy. One of the objectives in this research is to prove that, although these effects may seem small, they are an important part of the DRF because they are large enough to affect the accuracy of the inverse problem.
- G03 cannot simulate the complex geometry involved in the DRF where the detector source is not on a major axis of the detector. But, in the detector-source configurations that are different, the use of different distances would be advantageous. This is due to the fact that a 3rd variable for elemental composition is now available. It would also be useful in the area of oil well logging to simulate the detector-source configuration on the side of the detector.
- The non-linearity and the flat continua can be very easily put into the spectra of G03. CEAR has already demonstrated this (Gardner and Sood, 2004). The flat continua can be thought of as a sort of geometry factor. The flat continuum is easily explained by its flatness, and is shown in the last figure of the first chapter of this thesis. The flat continuum is caused by the escape of electrons from the sides of the detector. When the electron comes from either the photoelectric effect

or the Compton Scattering process, there are finite probabilities of distance out of the detector. Therefore, the effect gives an approximately flat shape because the electrons behave in an approximately constant $\frac{dE}{dx}$ relationship. This relationship dictates that the electron gradually loses its energy as a function of distance traveled. For example, the right side of the flat continua is demonstrated when a photoelectric effect happens near the corner and the photoelectron's trajectory takes it towards the opposite corner. And conversely, on the left side of the continua, when a photoelectric effect happens, and it is near the corner of the detector, the electron's trajectory is the smallest possible distance out of the detector, so it deposits very little energy. Straggling effects are the result of a process in which the electron trajectory has a tendency to be erratic. In actuality, electrons are either absorbed or scattered, which G03 is not considering. In the last chapter, the semi-empirical relationship that describes the electron transport is not based on this. This is a way to simplify and spend less money on computer calculation times because the complex electron transport that is employed in MCNP5 takes a factor of ten more times than when electron transport is not considered.

- Parts of the code were written in an f77 FORTRAN context; this is to be changed in all subroutines and main processes. This is done for practical efficiency purposes.
- A possible upgrade to MCNP search for cross section data, which is done in equation of the function in three detector's cross section acquisitions for the basic

photon cross sections, as well as the total of the three. This cross section protocol will be benchmarked against MCNP's cross section procedure. This can be easily explained as an analysis of functional vs. tabular.

- More modifications and notes to those modifications will be added to the code to benefit future code users.
- Does not include the natural radioactivity that some of the elements used in detectors have, such as lanthanum detectors. Note: this is a low energy, low yield effect as demonstrated in Figure 8. complements of (INL, Hartwell, personal correspondence supplied by Harp).

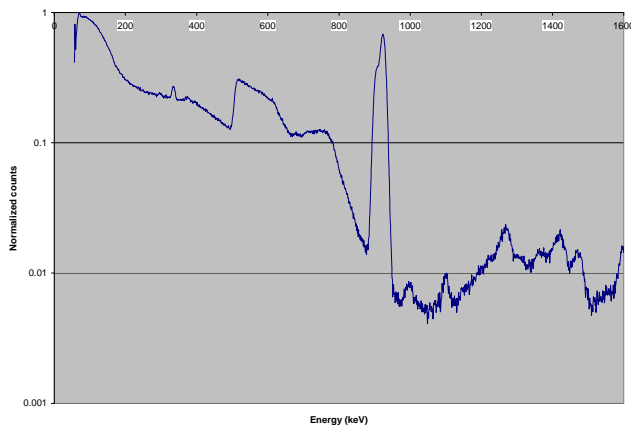


Figure 8: Background of radioactivity coming from the lanthanum part of La_3Br

- G03 is limited to only simulating NaI, and no other types of detectors. No high resolution scintillation detector data is available at the present time, and at high energy This is due to the fact that higher order interactions need to be added like photonuclear and triplet production.

- Detector size, at present, has been limited to 3 X 3 and some 6 X 6 simulations.

There is no flexibility to go to other sizes or shapes at this time.

4 MCNP Simulation of Can Phenomena

At this time, we decided to run an investigation of what exactly the detector can contribute to the spectrum. The source was used isotropically but, in order to save time, the tightest geometry was employed. The MCNP universe was shaped in a cylinder with the diameter just larger than a typical 3x3 NaI detector and as long as the length of the detector plus 10 centimeters. The extra 10 centimeters is used for the source that is aligned on axis with the detector. The first simulations were with no detector protective can (WOC), with the front of the can only (WC), and with the can on the detector (WWC). The detector specs were given in Heath and are shown below in figure 9. As shown below, the front of the can has four layers, while the side of the can has only two and is 36% less thick than the front. It is important to note that the higher atomic Z number, meaning more protons are present, the higher the probability of interaction with the side of the can which is important when Neoprene Rubber is present. It is composed of a little hydrogen, with 52% by weight Carbon, and very near 40% by weight Chlorine, comprising a moderate Z material, which will propagate more Compton events.

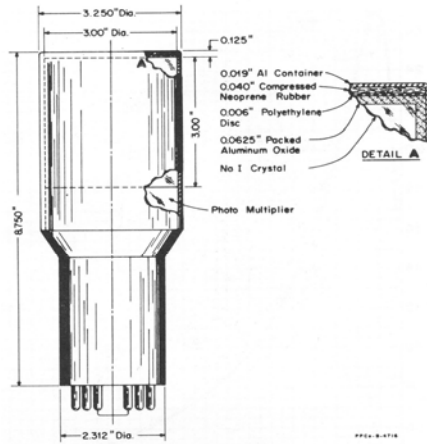


FIG. 39 - Typical commercial scintillation detector (3"x3") showing details of packaging technique. The increased mass of material used in the packaging of these detectors will produce some distortion of the spectrum due to scattering.

Figure 9: Heath can schematic. (1964)

The three simulations were run in order to find what the detectors affect in the can that has been stated earlier in Sood and compensate for the difference in the valley region. Is it the electrons or photons in the front of the can? Or maybe other parts of the spectrum's variability can be attributed to the can on the side from photons bouncing back in from a Compton? Or electrons staggering in and out of the can into the crystal. At this point, only a surface tally was performed between the front face and the front of the crystal. This is because it was hypothesized that this was the dominant effect that was affirmed in the Sood Thesis (2000). The pulse height tally also runs for the three simulations. Also later in order to be sure an electron current tally was employed at the can crystal interface. All the detectors were run at 27 different energies from 0.01 to 10 MeV. This is cataloged as an unspread MCNP detector response function.

These results show that it is indeed the front of the can that contributes to the valley region difference. Also, in all the different detectors, a kind of backwards

continuum in the Compton range is present. The “edge” is in the same energy for all of the different simulations for different detectors, and at different energies. One way to explain it is to say that the detector can side provides a specific backscatter into the continuum were this energy is located.

Into the investigation of the input file, the photopeak was found as a function of energy to be as much as 94% of the total spectrum, which is shown below in Figure 12.

This could explain the valley region seen in Figure 13. This is a spectrum of the photons actually striking the crystal, after they have been attenuated throughout the can. Figure 14 shows further interesting results. The graph states that many photons are attenuating through the can and spreading throughout the spectrum. This causes a sizeable difference in the valley region, which can be explained as many different photopeaks in the valley region, due to Compton Scatters. This is shown in Figure 13 at the five low energies, with same the 3x3 NaI detector. We also obtained the electrons from the three basic interactions, which will affect the spectrum. This is shown below in Figure 14.

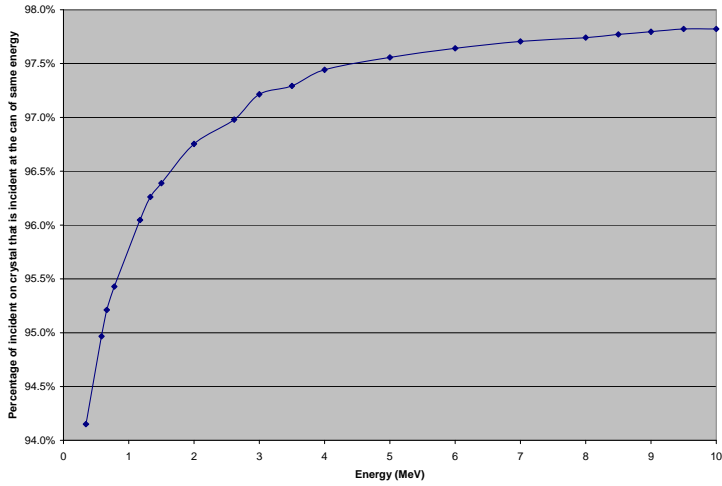


Figure 10: Percentage of photons going through the front of the detector can that are not being attenuated for Heath 3x3.

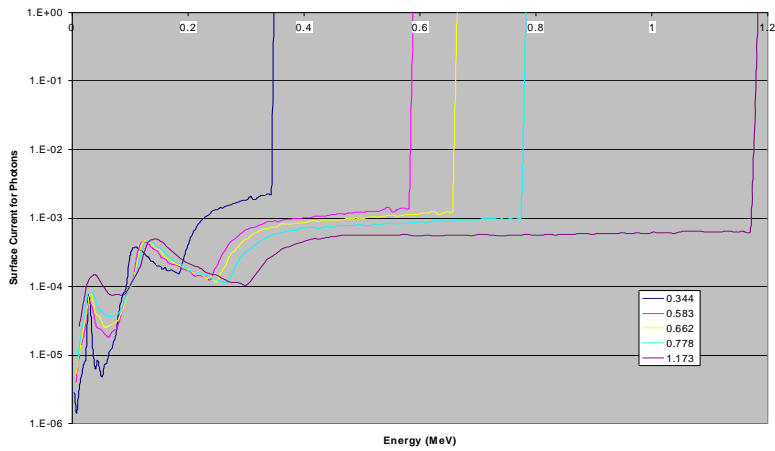


Figure 11: Photon spectrum incident on the crystal after being attenuated through the can.

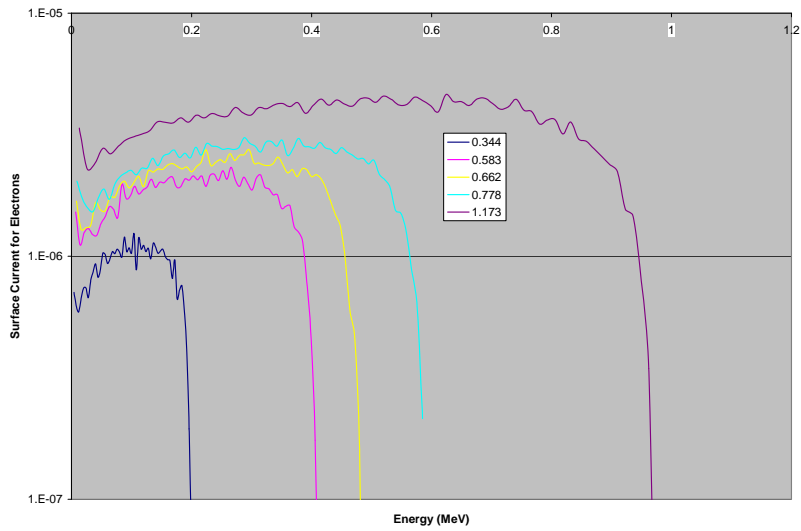


Figure 12: Electron spectrum incident on the crystal after being attenuated through the can.

The analysis of some of the MCNP output yielded showed interesting results. It showed that the side of the housing, or can, might actually be caused not from the front of the can but the side as shown in figures 13 and 14.

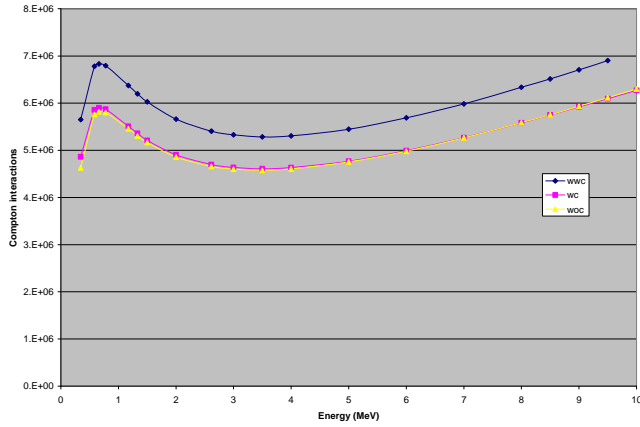


Figure 13: Compton interactions with the whole protective can (wwc), without the can (woc), and with just the front face (wc).

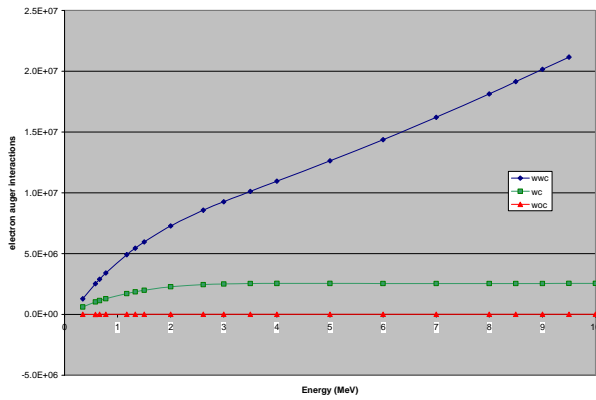


Figure 14: Auger electron with the whole protective can (wwc), without the can (woc), and with just the front face (wc).

The results are shown below in figures 15-17 for NaI, BGO, and La₃Br detectors which were run for comparison. The difference between the simulations of the one with the front of can and the whole can show the effects can be shown in the Compton Continuum. It is important to note that this is the unspread of the Gaussian data. This

simulation assumes a perfect crystal with no defects. The detector's imperfection in non-unity ratio to energy deposited to charge collection is the non linearity and a function of peak shift and the non linearity. Since it is a perfect detector, one can observe the X-rays from the higher Z constituents of the detector crystal.

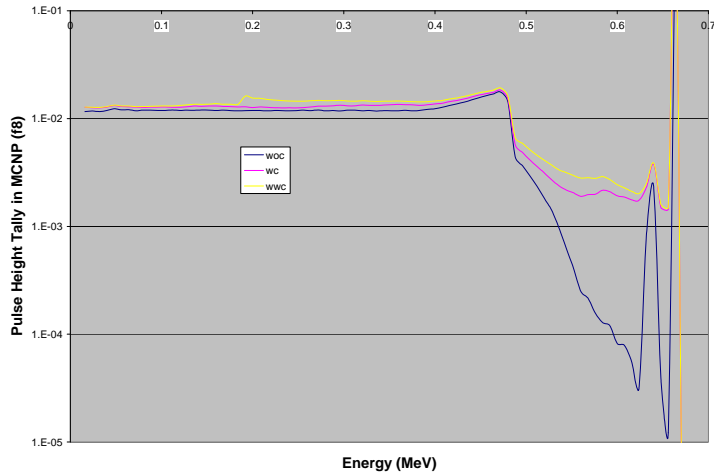


Figure 15: NaI Unspread spectra.

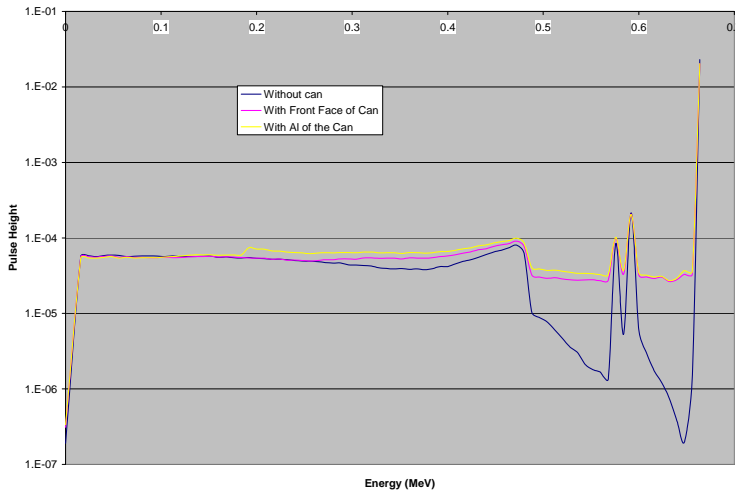


Figure 16: BGO Unspread spectra.

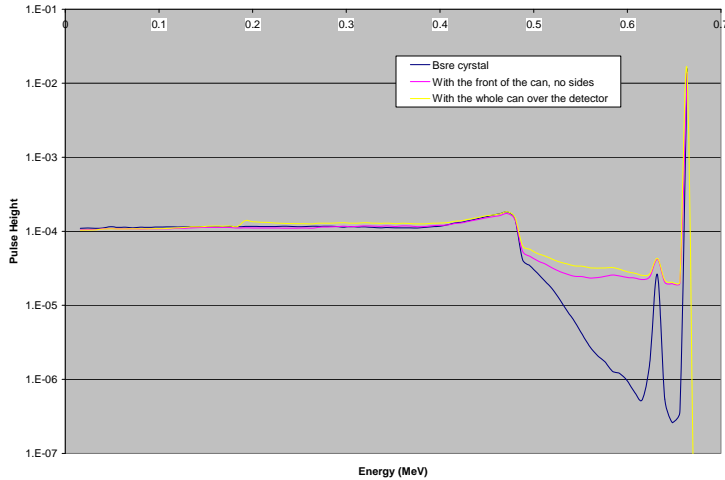


Figure 17: LaBr Unspread spectra.

This data represents a preliminary investigation into how the can affects the spectra. Now, if we are to implement it into G03, some things need to be done, in order to fully add the contribution to the can:

1. The spectra that needs to be interpolated needs to have the same number of channels regardless of energy. This was not done earlier; instead the simulations had 256 channels across the whole energy range, which was different depending on the energy studied. For these later simulations, there were 1002 channels spanned from 0 to 10 MeV
2. The contribution to the outside of the can needs to be documented for both electrons and photons. The reason for this documentation is clearly illustrated in figures 15-17. The spectrum, with only the front face of the can, was lower in the Compton Continuum than the simulations for the whole can for all three different types of detectors. There is a place, if one investigates those figures, in the

Compton Continuum where there is a “backwards” continuum. It is at the same energy for all three different types of detectors. Effectively, this means that this is a direct function of the composition of the can. G03 is based on the Heath data, and other detectors might not be represented here perfectly. It is important to note that this is an approximation, acknowledging that some photons can scatter out, and then back inside.

3. Investigate the possible contribution of the PMT-detector interface to the DRF.

Some of these goals that were put in place for MCNP were hard while others were easy. The first goal was easiest because all that was necessary was change a couple lines of code. Number two was relatively easy, but number three took a great deal of effort. The problem is that MCNP does not have surface treatment explicitly for a curved surface like it does for the flat surface. This is because the flat surface can easily be divided up into out or in the Cosine being positive or negative, which is the command in MCNP. To define a Cosine angle for a curved surface is not done in MCNP. So, with some help from my colleges, a strategy was employed to get the flux of the outer can. Two decks were run, one with and one without the detector can, rather than the three described earlier. A surface flux tally was obtained from these two. And then the tally of the one without the can was subtracted from the one with the can. Again, it is important to note that this is an approximation. This is due to the fact that there are some interactions where a photon can bounce back and forth between the crystal and the can, and affect the accuracy of this number. Then the spectra needed to be multiplied by the area of the cylinder part of the

detector can. This was done in order to obtain the per source particle representation of the current coming back into the can for the photons. The results of this are shown below in figures 18 and 19, for the lower energy runs. And, in figures 20 and 21, are the results of the attenuated current that strikes the crystal from the front.

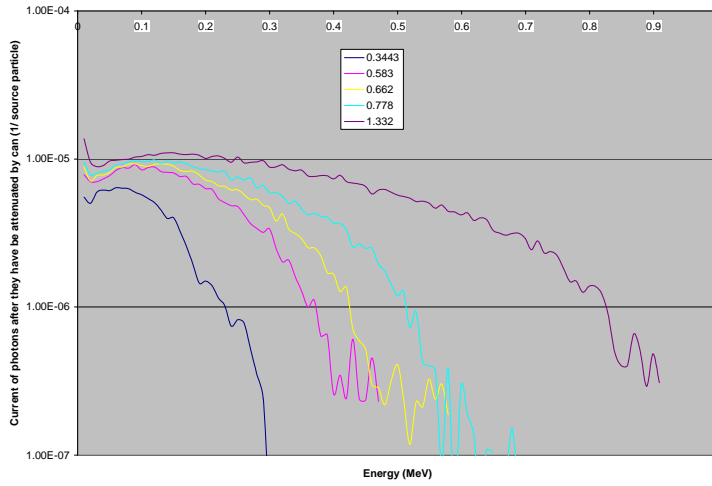


Figure 18: Electron spectrum bouncing back into the detector from the side.

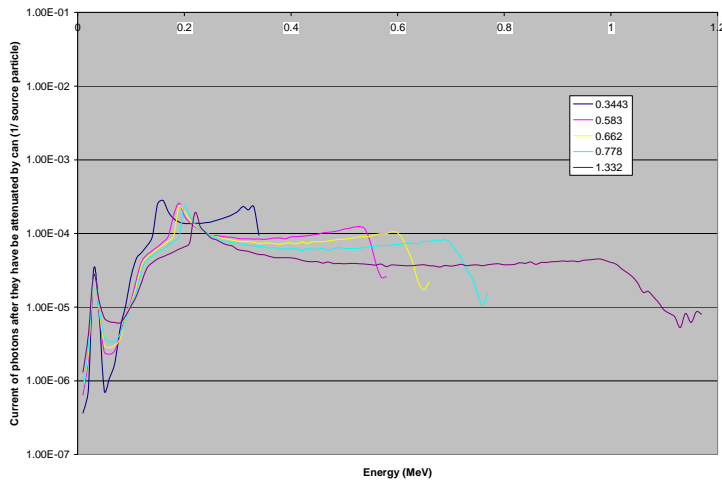


Figure 19: Photon spectrum bouncing back into the detector from the side.

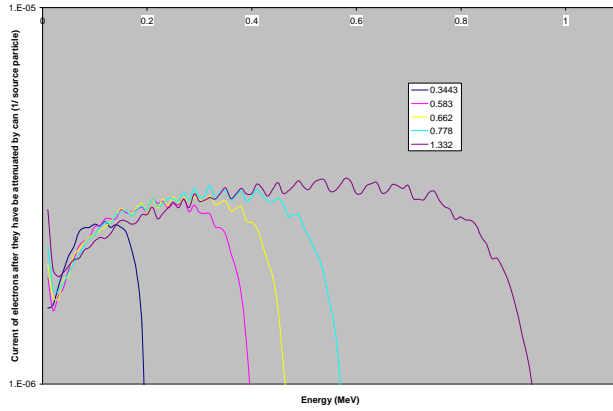


Figure 20: Electron spectrum incident on the crystal after being attenuated through the can.

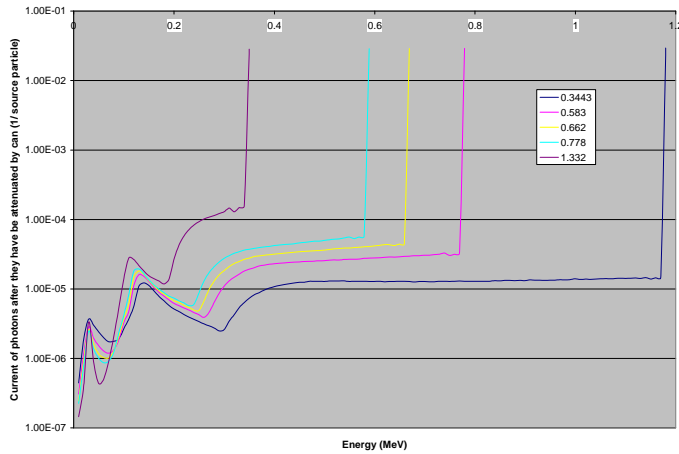


Figure 21: Photon spectrum incident on the crystal after being attenuated through the can

In addition to comparing G03 with Heath, CEAR wanted to benchmark against other types of detectors. The detectors that were considered included St. Gobain's 2x2 NaI, BGO, and LSO. These were all wrapped with Teflon in order to keep the important hydrostatic condition of the crystal intact. Padding is put at the top to prevent chipping of

the crystal. Then, everything is surrounded by Aluminum. Also included is a plastic box scintillator that is 2"x12"x12" in volume, which is needed for the DRF for CEARCPG. The theory is that coincidence counting would be more efficient for a detector that has a massive volume. All the detectors were simulated for 7 energies up to 2.614 MeV, 10 cm from the front of the detector and all the tallies obtain basically the same thing: the photons coming back into the detector. For the box detector, only the whole can needed to be simulated because we do not have the curved surface problem that we had for cylindrical detectors. The Homeland Security detector is a 16"x4"x2" NaI detector from St. Gobain and shown in figure 20. The box detectors were simulated on the widest surface area side, which is the way it is employed in the field to maximize efficiency. The big difference is that electrons were not simulated because the low yield and hence negligible contribution to the response. The cylindrical detectors, shown quantitatively in Figure 21, are all assumed to be the front.

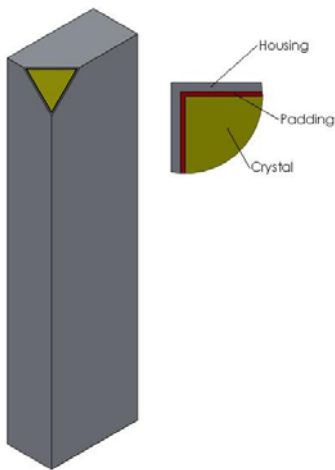


Figure 22: St. Gobain 16"x4"x2" NaI Detector (produced by Holmes)

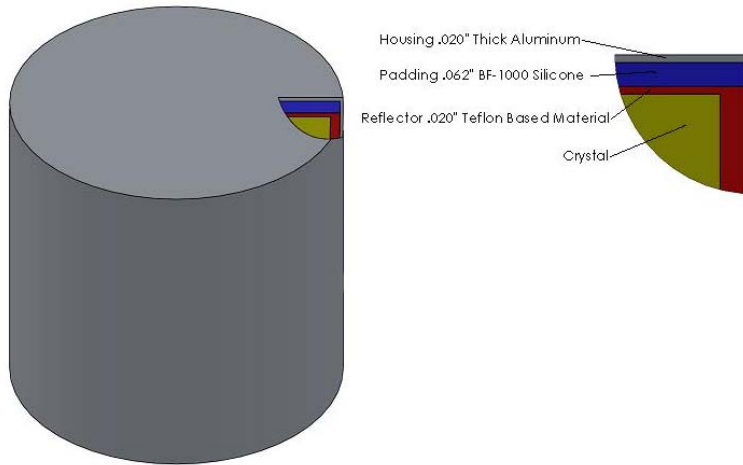


Figure 23: Typical Detector Housing for all produced 2x2 Cylindrical Detector
(produced by Holmes)

5 Implantation of Simulated Phenomena into G03

The primary purpose of this project is to implant all of these effects into the existing G03 code and then see if the spectra would be more representative of what happens in the can. The biggest contribution comes from the photons that go through the front of the can. This part is essentially a detector response function within itself. This is because what is actually hitting the crystal is several monoenergetic photons hitting the crystal, at different yields, and adding those responses to get the spectra that should be seen in the experiment.

To accomplish this feat, it is done very similarly to that described above. From Chapter 4 we have the spectra per source particle entering the front of the can for 20 monoenergetic photons. With this data we can 3 dimensionally obtain the spectra for any energies between 0.01 and 10 MeV. This 3-D universe has the 3 axis of: (1) Energy of incident photons on can- E , (2) Attenuated photon energy- E' , and (3) Tally as function of $f(E,E')$. In order to simplify the use of three 3-d full interpolation the functions of $f[E_N, f(E, Tal)]$, which is a fancy way of saying for every incident energy on the can there is a spectrum that can be represented in a piecewise graph. The point in which G03 calls its energy which is monogenetic in each spectrum, which is the inter loop of G03, it goes through this interpolation.

Another way to keep G03 moving faster is to do a post-processing step instead. figure 24 below is the photon spectra (normalized to unity) after it passes through the protective can for one of those energies, cesium energy in this case. The plot can be seen as an elemental abundance for each of these points are monoenergetic energies hitting the

crystal. The reason why it is normalized is when the can spectra hits the crystal all the appropriate weights for the geometry factor have been accounted for in G03. Otherwise, the photon flux incident of the can/crystal interface. It looks like the photopeak energy is unity, but it looks close to it on a semi-log graph. For Cs we have 95.1% uncollided flux. The rest is just 4.9% of the spectra but it is deposited throughout the spectra. To add the can contribution in a simple way is to treat each one of these points as the spectra of certain abundance. So then, the unspread, non-linear library with the light yield included is multiplied channel-by-channel and simultaneously added together to obtain the total spectra. The unspread data needed to be obtained, and is shown in figure 25. The result of this is spread so instead of many peaks, it will smooth out and have a flat continuum, due to majority of the continuants, again 95.1%. Then the spread is then applied which changes the bums from all those monoenergetic spectra will sooth out.

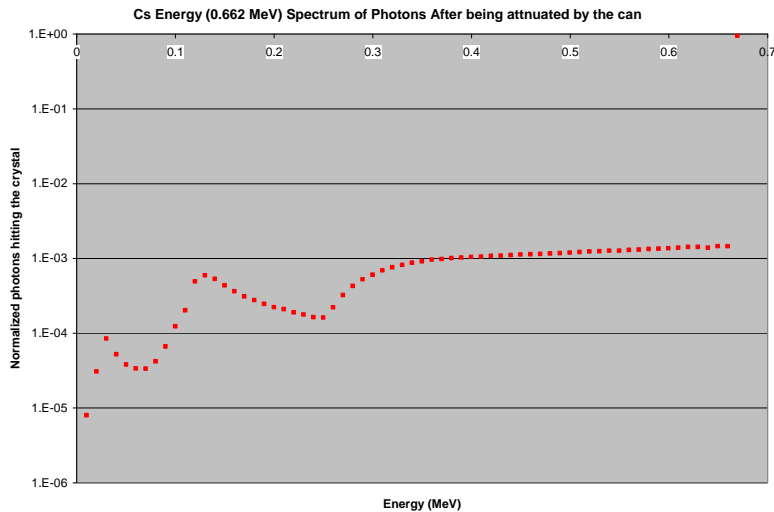


Figure 24: Cesium spectra point wise after attenuated through the front of the protective can

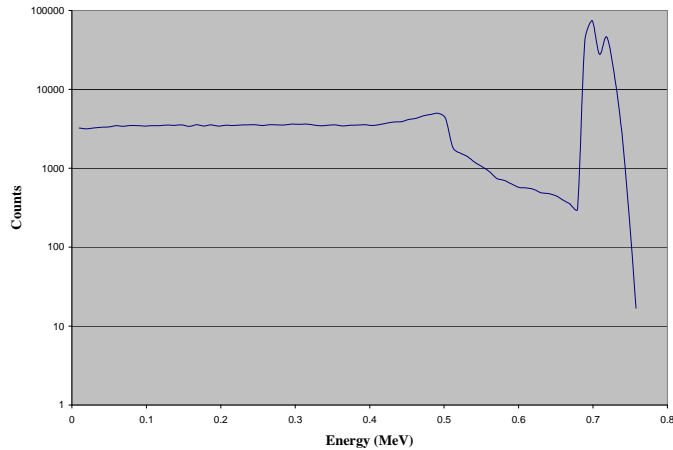


Figure 25: Unspread spectra for Cesium Unshifted spectra from G03

The same can be accomplished with the side of the can contribution, which is responsible for the backwards continuum, previously shown in chapter 4. This is the difference between the detector with its whole protective housing, the second with the front face of the cylinder being covered, and the third being with the bare crystal.

The way that the photon contribution from the side of the can. Discussed earlier, this happens when an interaction brings the incident photon back into the can. The process of deduction is Compton, Pair Production from the anti-annihilation photon, and secondary interactions. In order to conserve yield the per-source particle the spectra will be maintained, with no normalizing. Let us say for instance that there is a G03 run done with 70,000 particles per spectrum. The spectrum of Indium would have the addition of the photon side run in MCNP. This is done in a per source particle per source particle addition to the spectrum. The fraction of the spectrum addition per source particle is shown in figure 24. This is the input probability for the MCNP deck which obtains the

earlier mention f8 tally. It is important to mention that the first or 0 channel or 0 energy probability in the MCNP will be unity minus the total of the spectrum below. In this way the per source particle will be preserved. If a G03 run is to run at the intermit spectrum of 0.662 MeV, which is on of the MCNP run detailed in chapter 4 of this work, and had 10,000 histories the addition from the electrons would be the spectrum in figure 26 times 10,000 for each channel. Now one can see how the backwards continuum is form as an addition to the spectra.

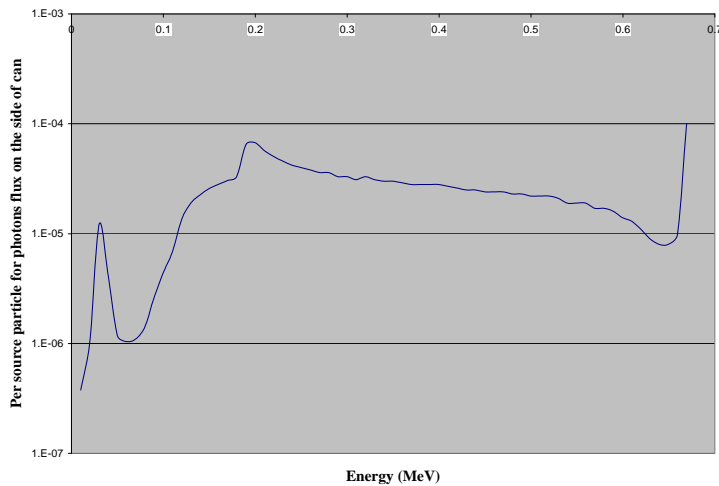


Figure 26: Per source particle of photons coming back into the crystal from the side.

Therefore, this work generalizes a DRF for any size type and shape, with a particular attention to contribution of the can. This was stated earlier apart of the detector response function because it is apart of the detector. To that goal a treatment has to be devised to address the variation of detector sizes first. A method was devised and implemented to use the Gaussian spreading parameters with differential operators. The

Gaussian parameters available in G03 are for 3x3, 3x6, and 6x6 detectors. The parameters that dictate the equation for the spreading is:

$$\sigma = aE^b \quad (5.1)$$

The parameters that are stated in Gardner and Sood are:

Table 1: Gaussian Spreading Parameters from the original G03

	3x3	3x6	6x6
a	0.0307	0.04009	0.02609
b	0.65934	0.36064	0.6027

Were differential operator come into play, that there is an assumption that there is correlation between the Gaussian parameters and physical dimensions such as volume, surface area, length, and radius. There are 3 different approaches that the author took to quantify this phenomenon:

1. Differential Volume:

$$(ab)_{n \times n} = \left(\frac{(ab)_{6 \times 6} - (ab)_{2 \times 2}}{V_{6 \times 6} - V_{2 \times 2}} \right) * V_{n \times n} \quad (5.2)$$

2. Differential Surface Area:

$$(ab)_{n \times n} = \left(\frac{(ab)_{6 \times 6} - (ab)_{2 \times 2}}{SA_{6 \times 6} - SA_{2 \times 2}} \right) * SA_{n \times n} \quad (5.3)$$

3. Differential Fundamental Dimensions:

$$(ab)_{n \times n} = \left(\frac{(ab)_{6 \times 6} - (ab)_{2 \times 2}}{D_{6 \times 6} - D_{2 \times 2}} \right) * D_{n \times n} + \left(\frac{(ab)_{6 \times 6} - (ab)_{2 \times 2}}{L_{6 \times 6} - L_{2 \times 2}} \right) * L_{n \times n} \quad (5.4)$$

where D is the diameter of the detector, L is the length, SA is the surface area normal to the surface at a set distance, and V is for Volume. The notation (ab) stands for either a or b as appropriate for a certain detector of equal diameter and length.

In order to further generalize a DRF code it was conceived that a box needed to be simulated. For practical purposes right now a box plastic scintillator and the St. Gobain Box detector is going to be benchmarked. The added flexibility was added to give any dimension at first at any distance normal to any surface. Then later the geometry option was added so that the source can be at any point or orientation, since they are mutually exclusive. Both programs or subroutines calculate the distance that a ray passes through a detector in a random fashion based solely on the random cosine angle. First, G03 calculates this distance of this ray for every particle initiated. Then the total cross section and type of interaction for that matter is calculated. Based on these two numbers a weight, and random interaction site is calculated. This is the reason why G03 is faster than MCNP in some ways. MCNP has to make a random choice at every surface were conversely, G03 is simple math and geometry simplification that is quite accurate. The necessary weights are calculated to the forcing of interaction into G03. So by its nature biasing is done so every particle hits the detector regardless of distance and every particle that goes into the detector has an interaction.

After that interaction, G03 calls another subroutine that calculates based on where the interaction happens moves the direction of the angle cosine, hence its trajectory, to the longest distance out of that detector. It does this based on the fact that in the cosine angles can be manipulated, in the plus minus sense, to have 6 variations in direction. This subroutine, called Travel, was developed by Douglas Peplow (Peplow, Gardner and Verghese, 1993) for the cylindrical case calculated the distance between the interaction site and the three surfaces, the two top discs and the periphery of the crystal. Then Travel subroutine forces the interaction to go to farthest distance plane, and calculated the crucial weights.

In the spirit of generalizing this code different materials need to be considered. As stated before the parameters are easy to manipulate. It is just finding the right place in the code, actually most of the time in the subroutines, to change it to represent the response for different materials. Electron Range relationship for other materials:

$$\frac{R_1}{R_2} = \frac{\rho_2 \sqrt{A_1}}{\rho_1 \sqrt{A_2}} \quad (5.5)$$

To accommodate the change of Bremsstrahlung in materials G03 weighting was shifted based on the actual Bremsstrahlung that NaI would cause. The ratio in the yields, like the ratio of range, are calculated and then multiplied in the weight due to the Z dependence:

$$Y = \frac{6 * 10^{-4} * ZT}{1 + 6 * 10^{-4} * ZT} \quad (5.6)$$

Where Z and A is effective Z and A, and respectively the effective number of protons or atomic weight, of detector crystal material. T is energy, ρ is density, and R is the Range of the electrons described earlier. Also the density needs to be implemented. The only

part were this is needed is the calculation of the flat continuum. This is because the density is imbedded into the cross sections of every material, which needs to be changed. The nonlinearity caused by the light yield, or electron collection efficacy, was added. This dramatically affects the actual behavior of the response. The relative light yield as a function is shown in Valentine et. al for NaI, LSO, and BGO detectors is shown below in Figure 27, and the light yield shown in Figure 28 is for LaBr.

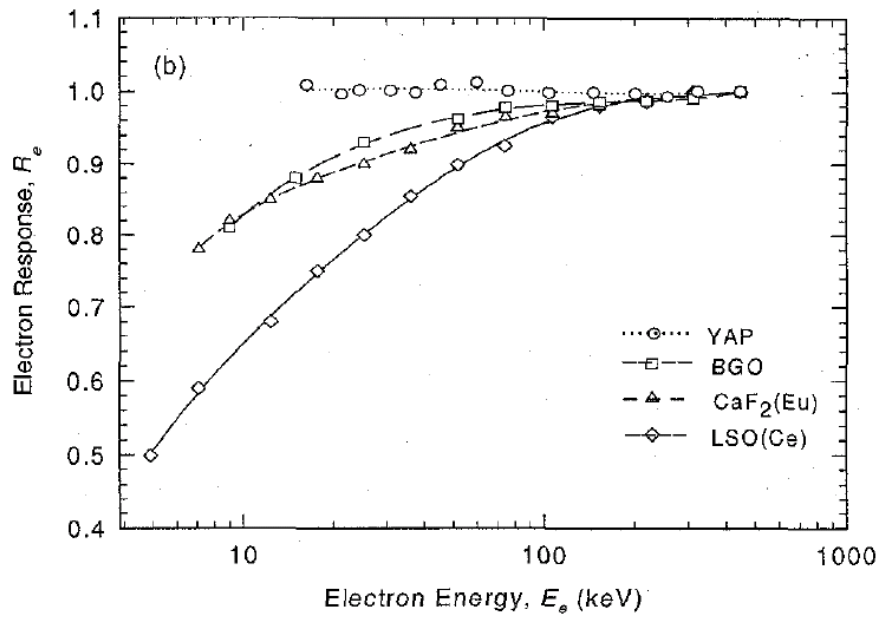


Figure 27: Light yield for various detectors. (Mengesha, Taulbee, Rooney, and Valentine, 1998)

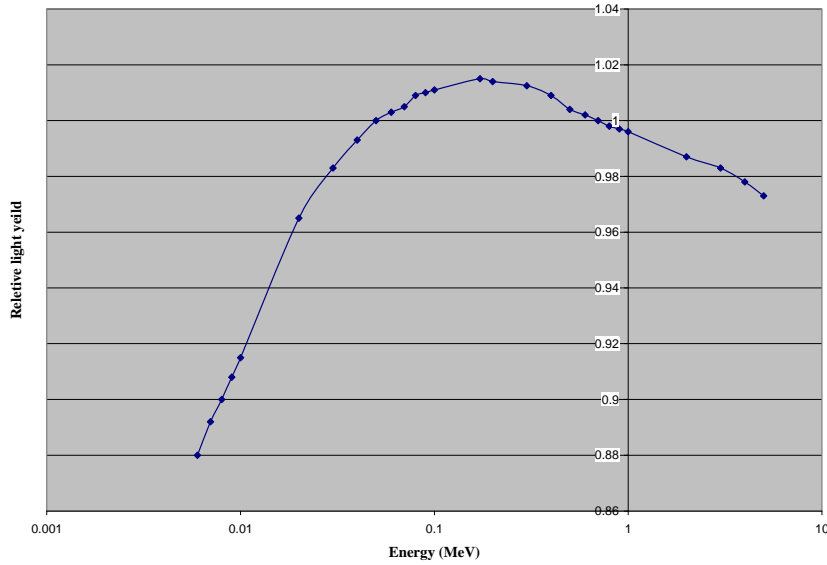


Figure 28: Light Yield for La_3Br

The first thing that was done to improve the time is the conversion of G03 from FORTRAN77 to FORTRAN99. The cross section treatments are a perfect example of this. One can do it like in G03, where the cross section is obtained in a functional form, but accuracy is not as good as it should be. Another approach to this problem is a tabular one like in MCNP. Unfortunately for MCNP time is sacrificed for accuracy, due to the fact of how tabular data is processed. Any searches through data no matter how proficient it has to first go through searching for the number of two energies that the energy in question that need to be interpolated, then interpolate. It has to interpolate because the probability of hitting a specific tabular integer for double precision is very low. In G03 the functional form eliminates the need of searches and secondary equations. If one puts in energy the output is the cross sections for the Photoelectric Effect, Compton

Scattering, and Pair Production. In turn, the total cross section which is the parameter that is needed in G03 for its preliminary calculations.

6 Results

6.1 Overall Statement of Detector Parameters and Preliminary Results

The results are from the cylindrical can compositions are shown in Chapter 2. The results are from the box detector compositions are shown in Chapter 4. The source-to-detector distance is 10 cm from the front of the can. Also different detector materials are shown. The variations that are not shown, but are also available are from the incident photons on the front and from the side, as well as electrons from the front and side. Also available but not shown is the case where the photon flux is going out the back hitting the PMT. The Box detectors were simulated with the source normal to the largest surface area and 10 cm away.

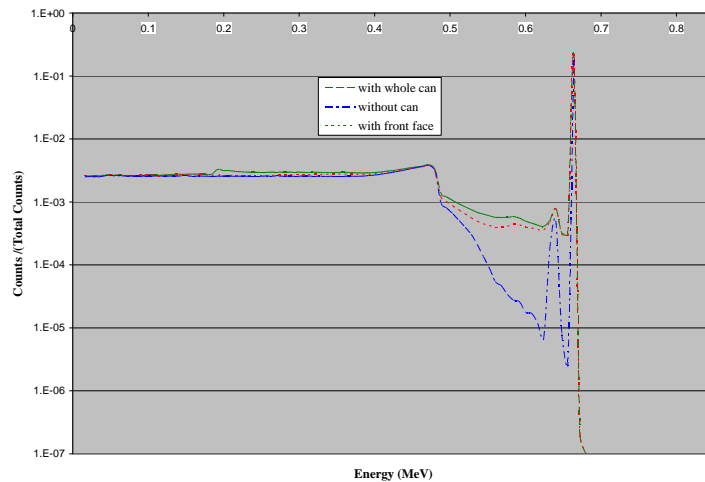


Figure 29: NaI 3x3 Heath 0.662 MeV

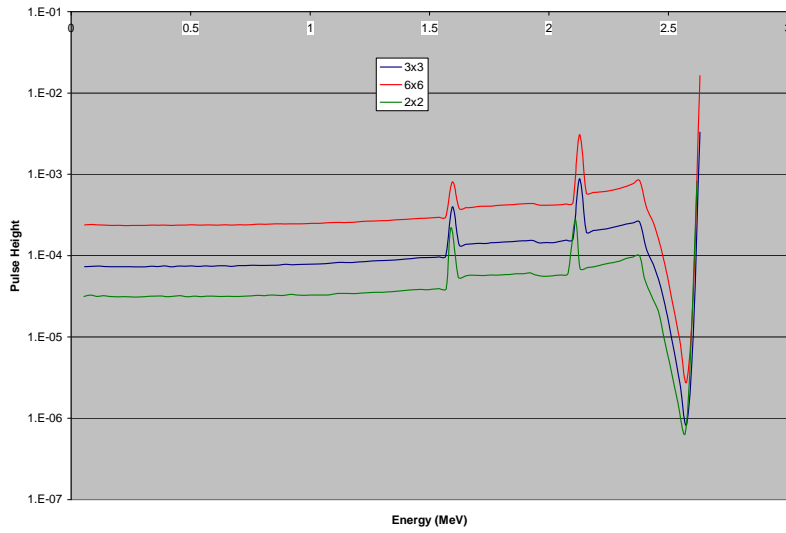


Figure 30: Heath can for different size NaI detectors Without Detector Housing for 2.614 MeV

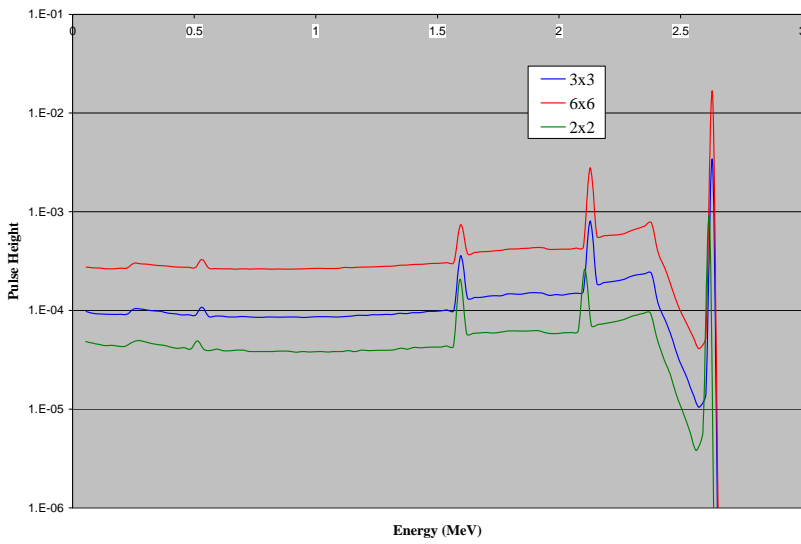


Figure 31: Heath can for different size NaI detectors With Detector Housing (Can) for 2.614 MeV

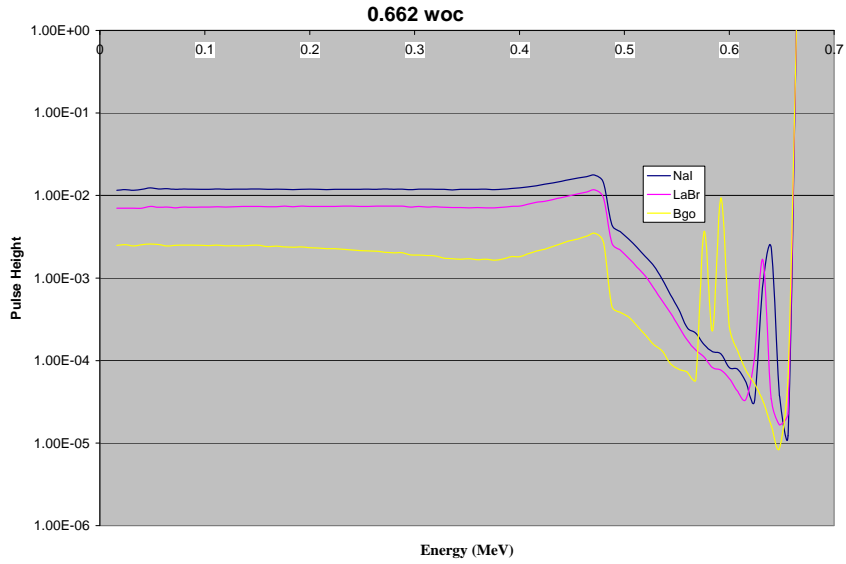


Figure 32: Without Heath can, different types of 3x3 Detectors for 0.662 MeV

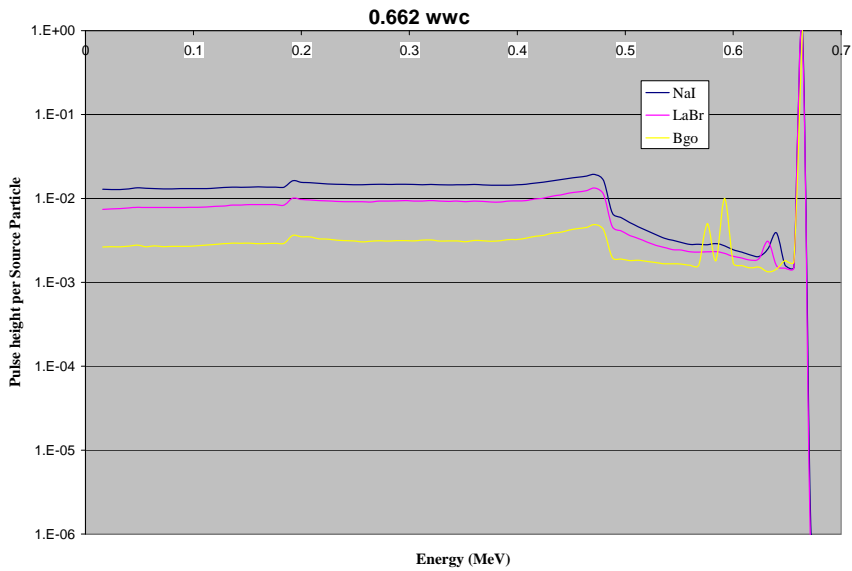


Figure 33: With Heath can, different types of 3x3 Detectors for 0.662 MeV

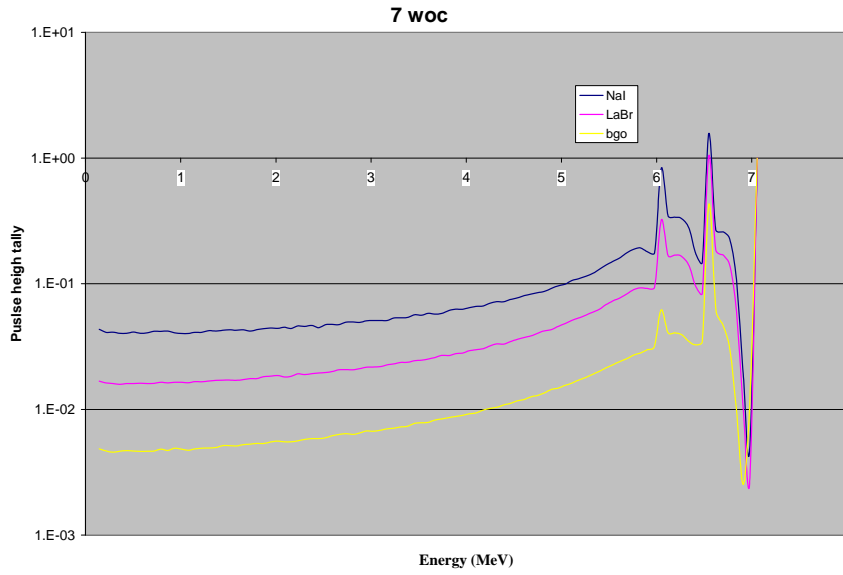


Figure 34: Without Heath can, different types of 3x3 Detectors for 7 MeV

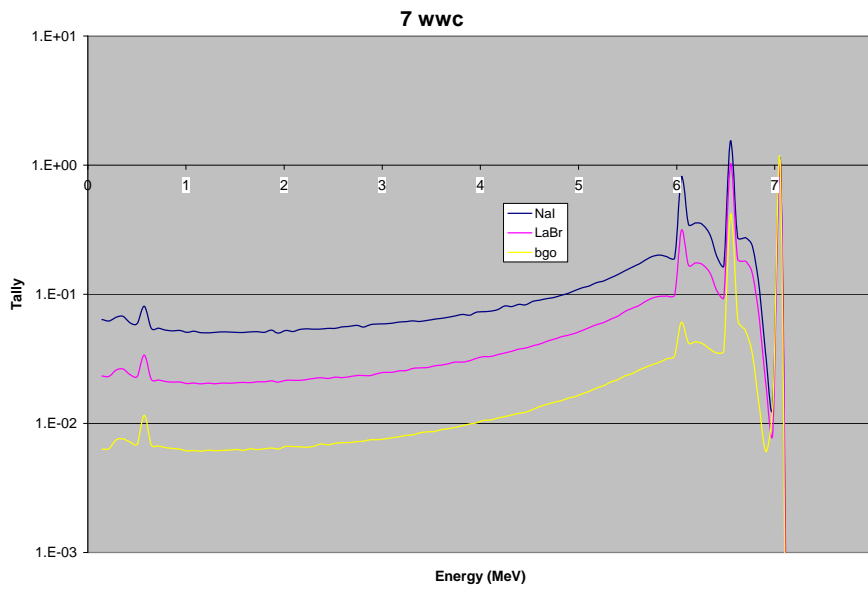


Figure 35: With Heath can, different types of 3x3 Detectors for 7 MeV

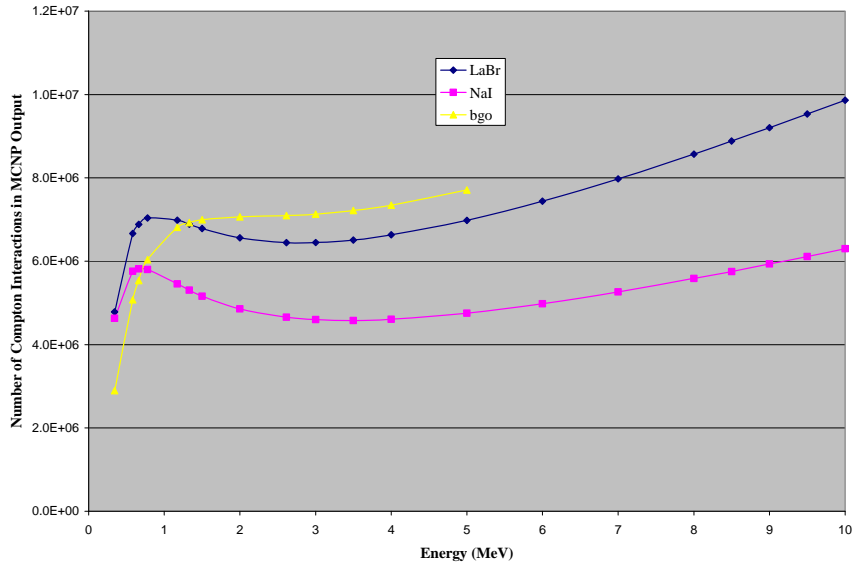


Figure 36: Compton interactions for various detector types, and without the protective can.

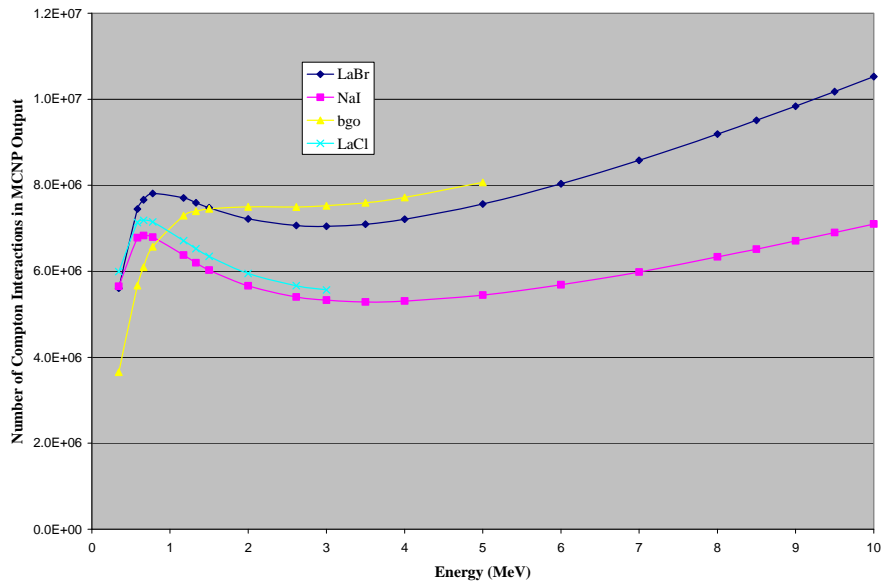


Figure 37: Compton interactions for various detector types, and with the protective can.

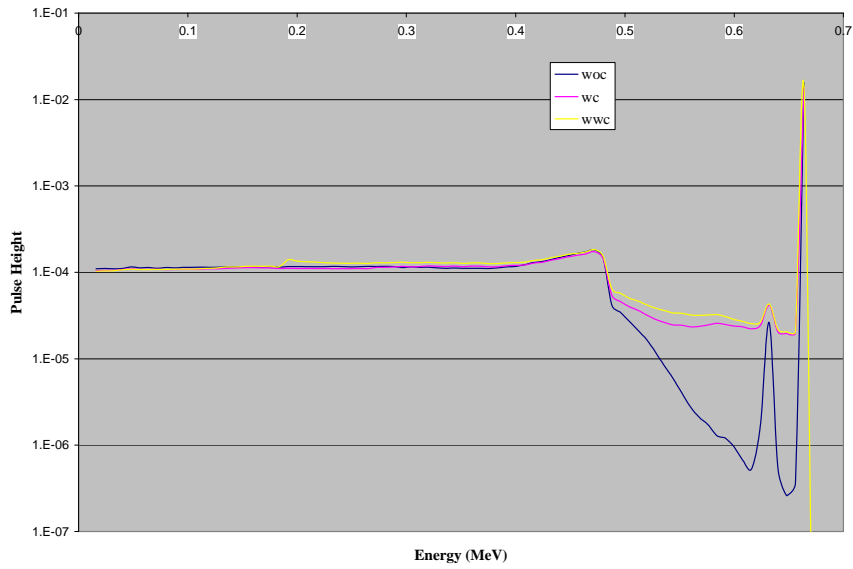


Figure 38: 3x3 LaBr detectors at 0.662 incident energy 256 channels with Heath can

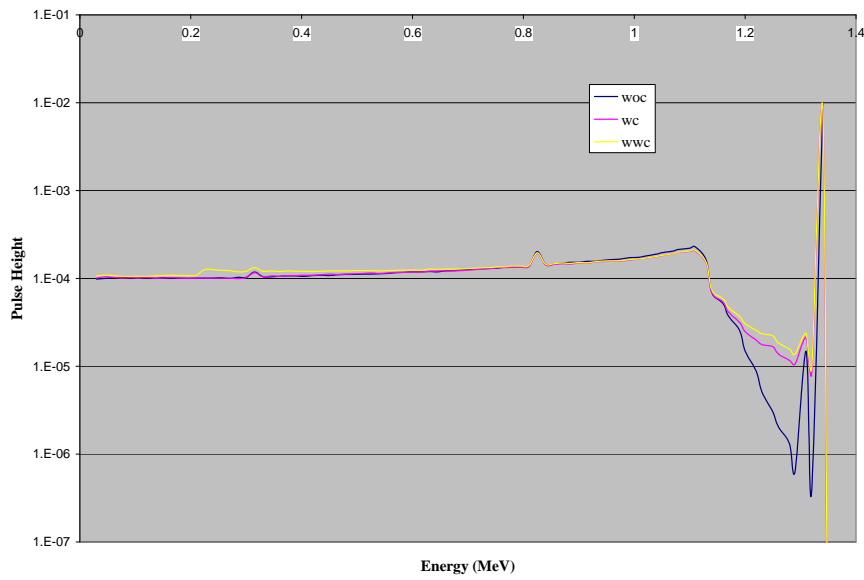


Figure 39: 3x3 LaBr detectors at 1.332 incident energy 256 channels with Heath can

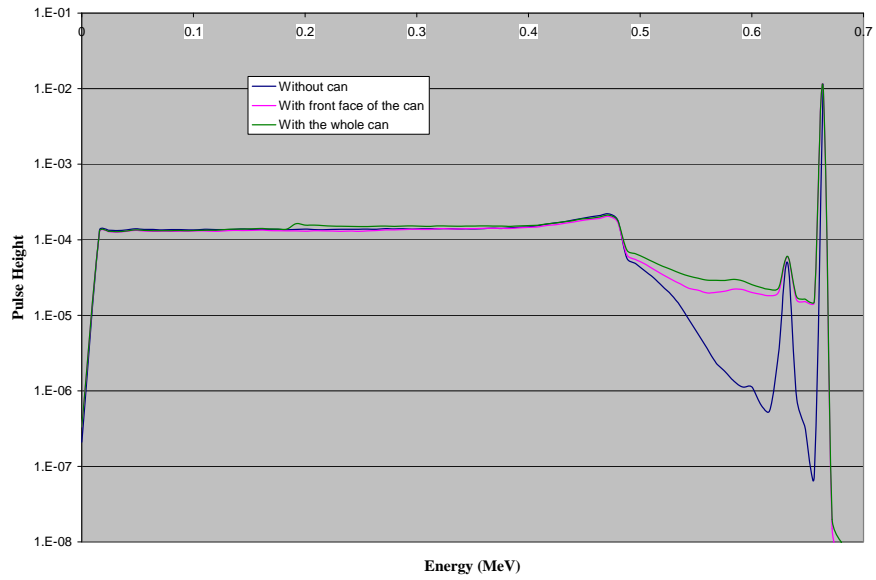


Figure 40: 3x3 LaCl detectors at 0.662 incident energy with Heath can and 256 channels

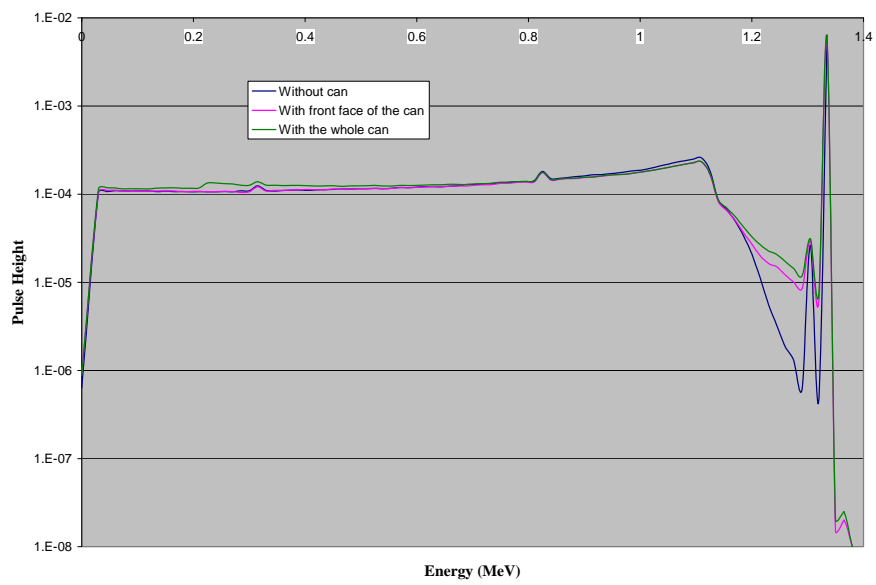


Figure 41: 3x3 LaCl detectors at 1.332 incident energy with Heath can and 256 channels

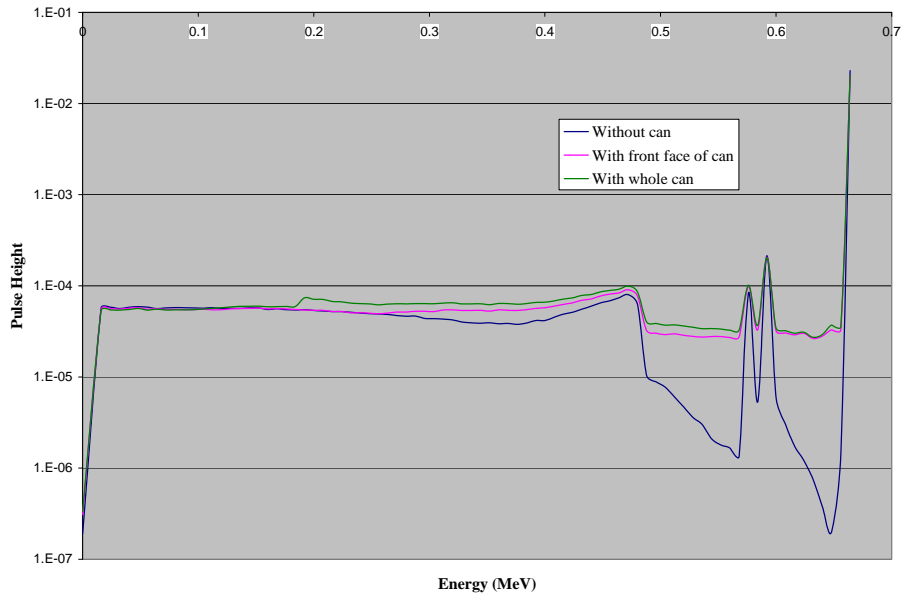


Figure 42: 3x3 BGO detectors at 0.662 incident energy

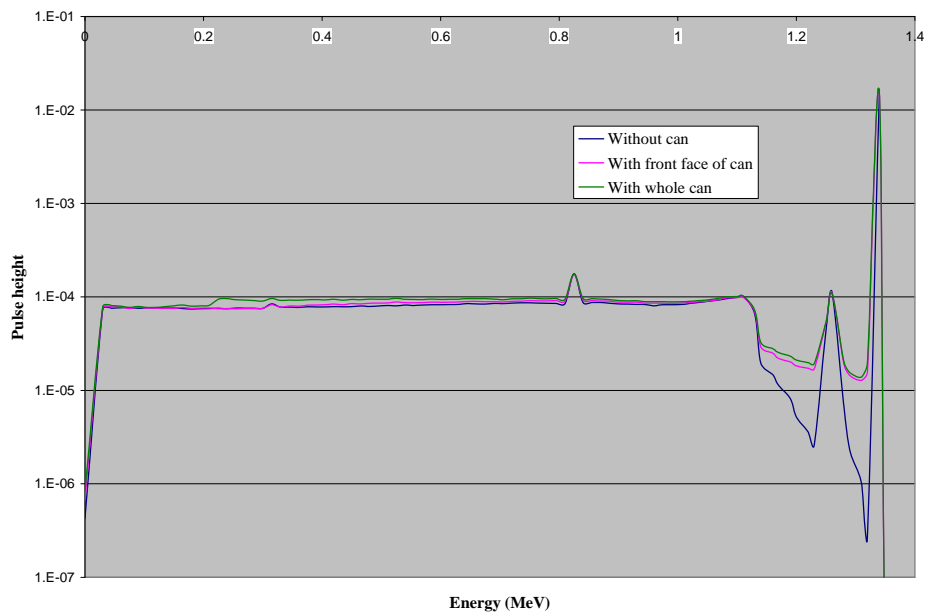


Figure 43: 3x3 BGO detectors at 1.332 incident energy and 256 channels

6.2 Heath can DATA final

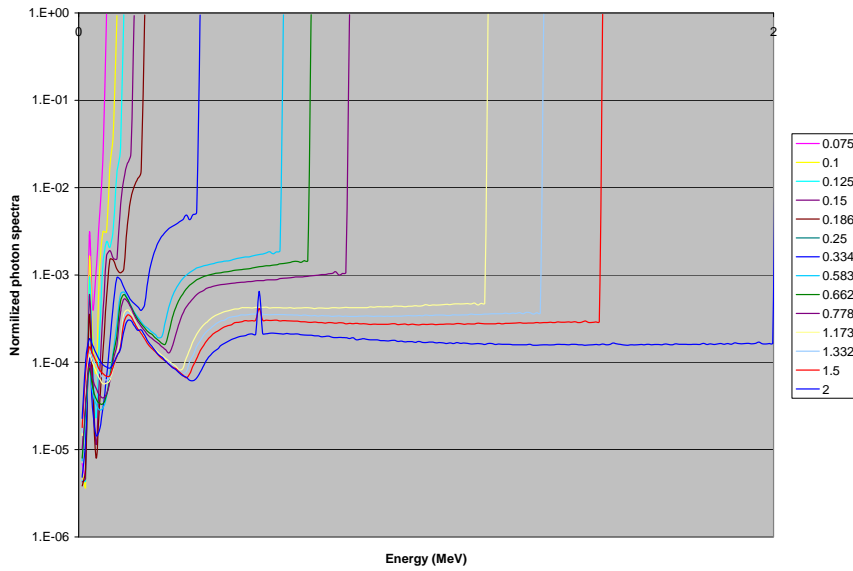


Figure 44: Photon front for 3x3 NaI 1002 channels with Heath can for selective energies for clarity

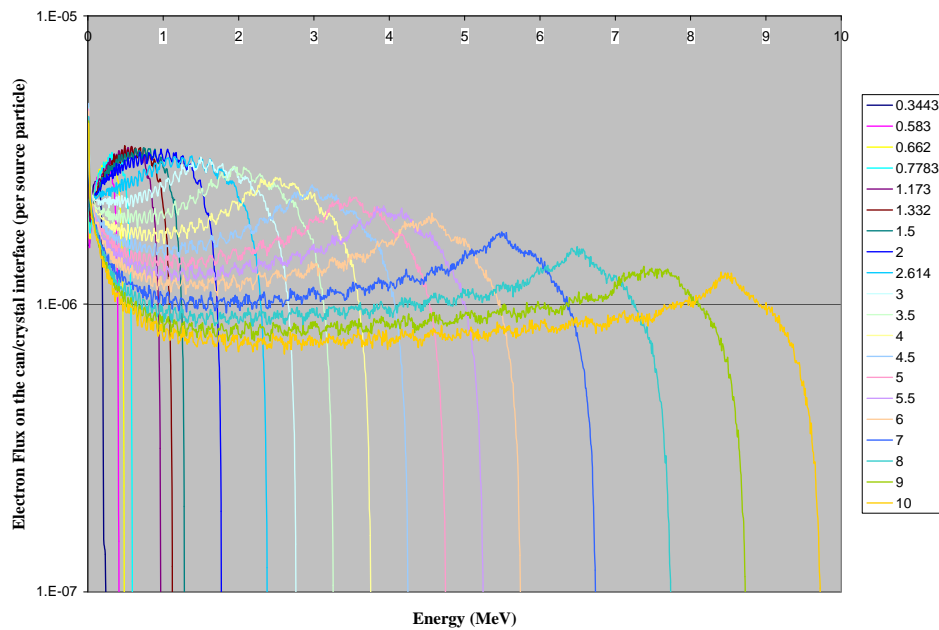


Figure 45: Electron Front for 3x3 NaI 1002 channels with Heath can

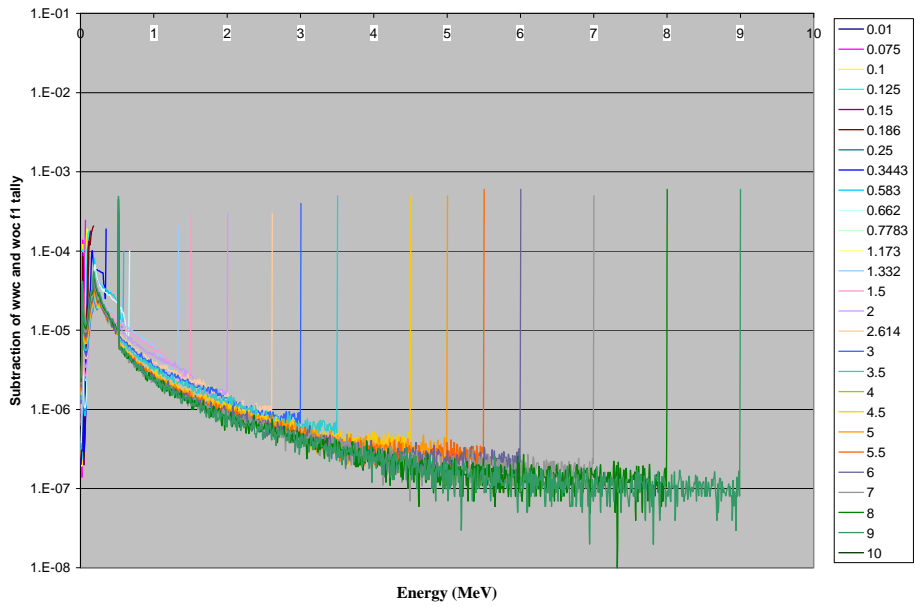


Figure 46: Photon side for 3x3 NaI 1002 channels with Heath can

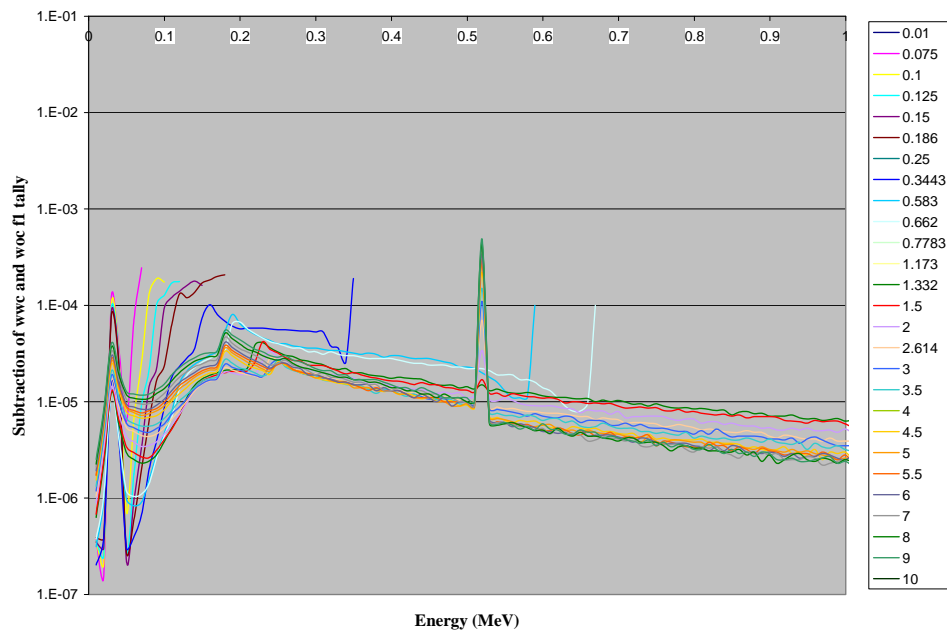


Figure 47: Photon side for 3x3 NaI 1002 channels with Heath can zoomed in

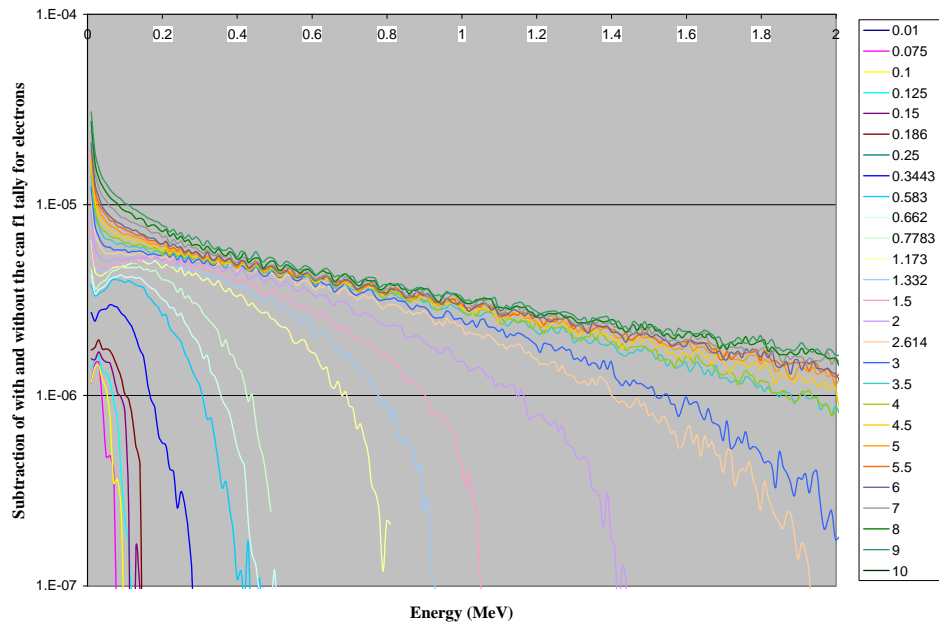


Figure 48: Electron side for 3x3 NaI 1002 channels with Heath can

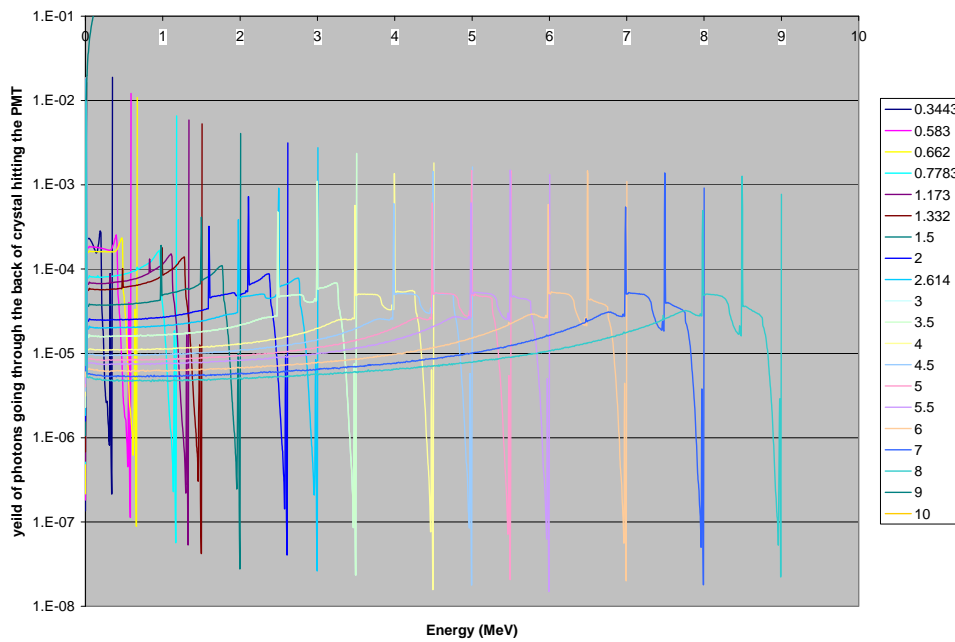


Figure 49: Pulse height with out can side for 3x3 NaI 1002 channels with Heath can

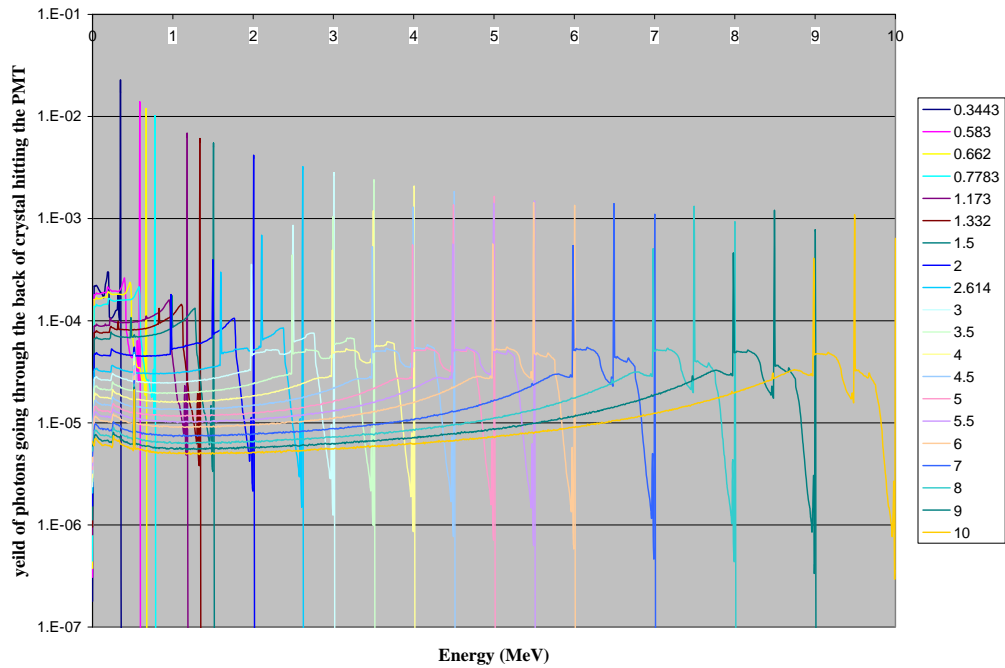


Figure 50: Pulse Height with whole can side for 3x3 NaI 1002 channels with Heath can

6.3 16"x4"x2" Sodium Iodine Portal Monitoring Detector

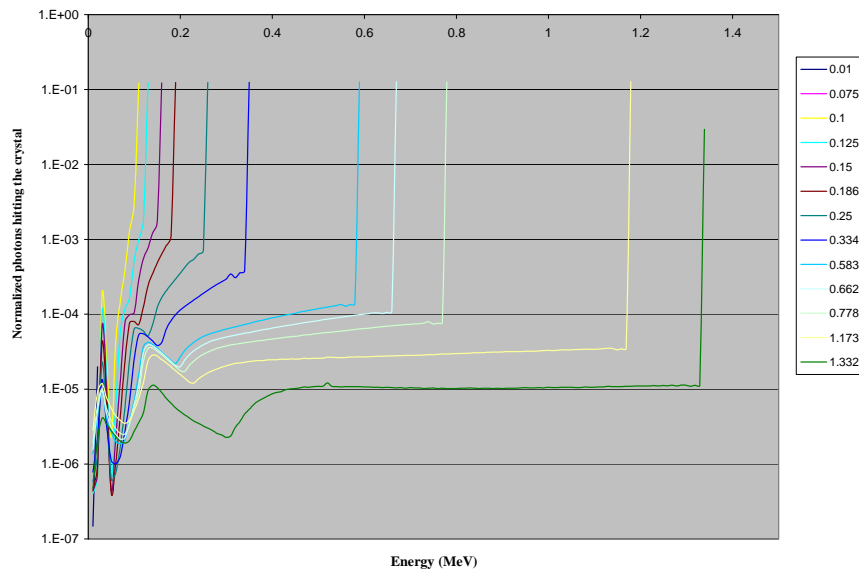


Figure 51: Photons in front for Raytheon box 16"x4"x2"

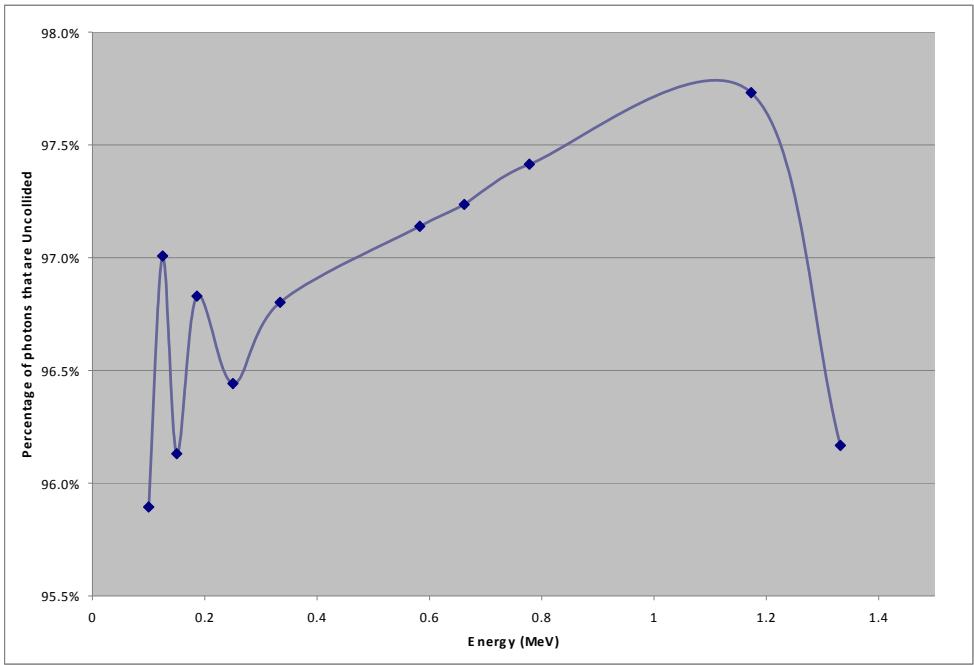


Figure 52: Percentage of uncollided Lux

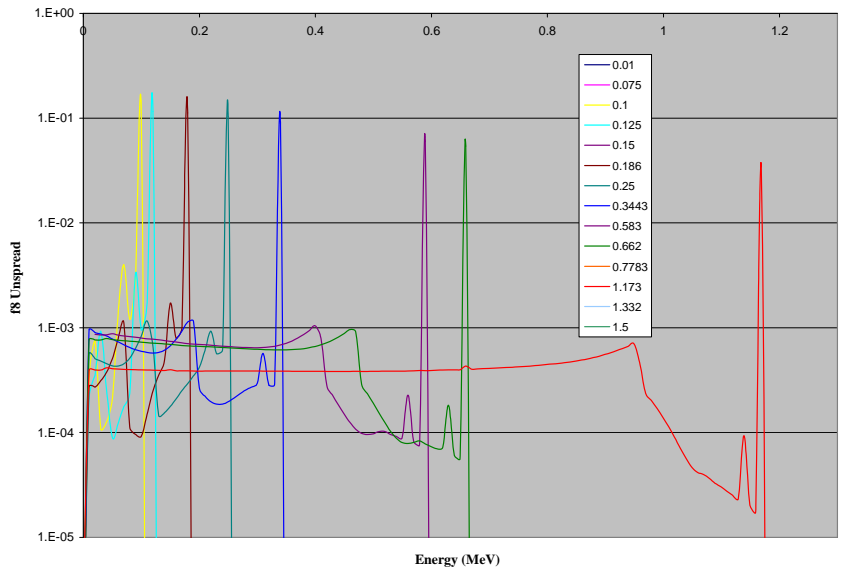


Figure 53: Pulse Height with whole can

6.4 G03 Results

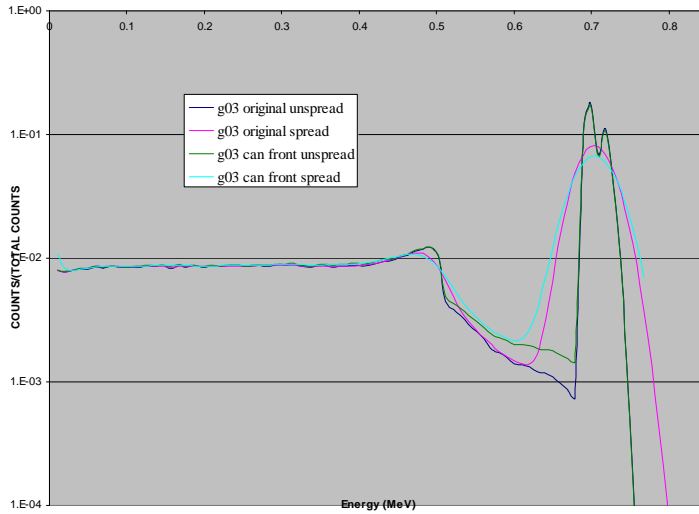


Figure 54: The affect of Photon spectra the pulse Height, and the showing of error in spreading the spectrum outside the code

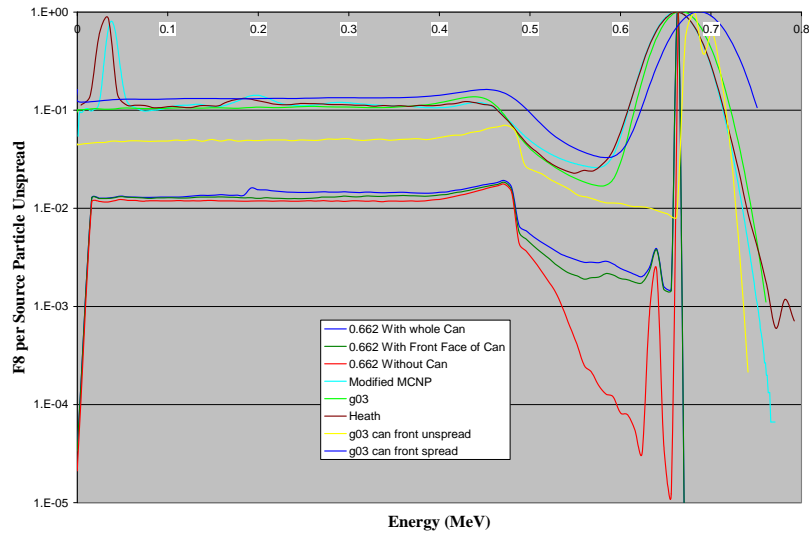


Figure 55: The affect of Photon spectra from the pulse height with MCNP and G03

7 Discussion and Conclusions

Many conclusions can be drawn using the application of the DRF in the Results section. There are several highlights to be remembered from the Results in regards to the MCNP simulations. One aspect of the simulations that was not included is the natural spreading done by the can, and/or binning effects from MCNP. The theory maintains that binning effects, the slight points on the right of the monoenergetic point, are of low value. It is also important to reiterate this thesis proves that the can constituents do affect a large part of the spectrum. If the monoenergetic energy is deposited across the spectra and across the rest of the spectrum, then dramatic results are seen in the differences in the Compton Continuum from both the side and front and the valley for the front of the detector can in the simulations run for this research. This addresses the sensitivity of the detector, which is probably the reason why detector companies are so hyper-conscious regarding other's knowledge of their detector compositions.

In closing, this thesis shows that the application and continual development of detector response function is actually an efficiency problem so it can always be improved upon. Four different detectors can be added with ease. Different sizes and shapes of detectors are now available in G03. Also, with this geometry addition, the radioactive source can be put any place in space. Cracks and impurities will affect the Gaussian parameters, electron range (due to electron channeling), and the relative light yield. Lower Z material such as Carbon fiber may be a better alternative than aluminum, especially for the high resolution detectors LaBr and LaCl.

8 References

- Berger M. J. and Seltzer S. M. (1972) "Response Functions for Sodium Iodide Scintillation Detectors," *Nuclear Instruments and Methods* 104, 317-322.
- Campbell J. L. (1990) "X-Ray Spectrometers for PIXE." *Nuclear instruments and Methods in Physics Research* B49, 115-125
- Doster, J. M. 1982, Ph.D Thesis, NCSU.
- Gardner, R. P., Metwally, W. A., Han, X. and Mayo, C.W. (2004) "Q-Value Summing for Coincidence Prompt Gamma-Ray Neutron Activation Analysis," *Transactions of the American Nuclear Society*, 91, 881-882.
- Gardner R.P.; Sood A. (2004) "A Monte Carlo Simulation for Generating NaI Detector Response Functions (DRF's) that accounts for the Nonlinearity and Variable Flat Continua," *Nuclear Instruments and Methods B*, 213, 87-99.
- Gardner, R.P. and Verghese, K. (1971) "On the Solid Angle Subtended by a Circular Disk," *Nuclear Instruments and Methods*, 93, 163-167.
- Gardner R. P., Yacout A. M., Zhang J. and Verghese K. (1986) "An Investigation of the Possible Interaction Mechanisms for Si(Li) and Ge Detector Response Functions by Monte Carlo Simulation," *Nuclear Instruments and Methods in Physics Research* A242, 399-405.
- Harp, J., personal communication 2007.
- He T., Gardner R. P. and Verghese K. (1990) "An Improved Si(Li) Detector Response Function," *Nuclear Instruments and Methods in Physics Research* A299, 354-366.
- Heath, R.L., 1964, "Scintillation Spectrometry," *Gamma-ray Spectrum Catalogue*, 2nd Edition, USAEC.
- Jin, Y., Gardner, R.P., and Verghese, K. (1986) "A Semi-Empirical Model for the Gamma-Ray Response Function of Germanium Detectors Based on Fundamental Interaction Mechanisms," *Nuclear Instruments and Methods in Physics Research*, A242, 416-426.
- Kahn H. (1954) "Applications of Monte Carlo," *USAEC Report AECU-3259*, Rand Corporation.

Knoll, G.F., 1989, "Radiation Detection and Measurement," John Wiley and Sons, Inc., New York.

Mattingly, J. personal communication 2008.

Mengesha, W., Taulbee, T.D., Rooney, B.D., Valentine, J.D. (1998) "Light Yield Nonproportionality of CsI(Tl), CsI(Na), and YAP," *IEEE Transactions on Nuclear Science*, 45, 3.

Mitchell, D. J., Sanger, H. M. and Marlow, K. W. (1989) "Gamma-Ray Response Functions for Scintillation and Semiconductor Detectors," *Nuclear Instruments and Methods in Physics Research*, A276, 547-556.

National Institute of Standards and Technology (1998) *Element/Compound/Mixture Selection*, from NIST XCOM website: <http://physics.nist.gov/PhysRefData/Xcom/Text/XCOM.html>

Pages L., Bertel E., Joffere H. and Sklavenitis L. (1972) "Energy Loss, Range and Bremsstrahlung Yield for 10 keV to 100 MeV Electrons," *Atomic Data* 4(1), 79.

Peplow, D.E. 1993, MS Thesis, NCSU.

Rowlands, G. (1961) "Solid Angle Calculations," *International Journal of Applied Radiation and Isotopes*, 10, 86-93.

Sood, D.E. 2000, MS Thesis, NCSU.

Sood, A.; Gardner R.P. (2004) "A New Monte Carlo Assisted Approach to Detector Response Functions," *Nuclear Instruments and Methods B*, 213, 100-104

Wielopolski, L. and Gardner, R. P. (1979) "A Generalized Method for Correcting Pulse-Height Spectra for the Peak Pile-Up Effect Due to Double Sum Pulses. Part II. The Inverse Calculation for Obtaining True from Observed Spectra," *Nuclear Instruments and Methods*, 140, 297-303.

Wieloposki, L. and Gardner, R. P. (1979) "Development of the Detector Response Function Approach for the Library Least-Squares Analysis of Energy-Dispersive X-Ray Fluorescence Spectra," *Advances in X-Ray Analysis*, 22, 317-323.

Yacout A. M., Gardner R. P. and Verghese K. (1986) "A Semi-Empirical Model for the X-Ray Si(Li) Detector Response Function," *Nuclear Instruments and Methods in Physics Research* A243, 121-130.